Leachate Experiments to Evaluate Weathering of Waste Rock for Backfill Aquifers in Restored Open Coal Mine Pits, Powder River Basin, USA

A Thesis

Presented in Partial Fulfillment of the Requirements for the

Degree of Masters of Science

with a

Major in Geology

in the

College of Graduate Studies

University of Idaho

by

Julianna M. Martin

Approved by:

Major Professor: Jeff Langman, Ph.D.

Committee Members: Jeff Langman, Ph.D.; Daniel Strawn, Ph.D.; James Moberly, Ph.D.

Department Administrator: Alistair Smith, Ph.D.

August 2023

Abstract

Open-pit mining companies utilize waste rock for landscape restoration which may include the construction of backfill aquifers. Chemical weathering and contaminant transport can be altered in backfill aquifers because of the mining of the waste rock that produces newly available mineral surfaces and nanoparticles that can impact water quality. Waste rock from the Cordero Rojo open-pit coal mine in the Powder River Basin was exposed to benchtop weathering experiments for 20 weeks at temperatures of 5 °C and 20 °C. Leach columns containing 4 kg of waste rock were saturated and drained twice weekly. Collected leachate was analyzed for Eh, pH, alkalinity, specific conductance, and cation and anion concentrations as unfiltered and 0.45-µm and 0.2-µm filtered concentrations. During the experiment, leachate Eh and pH substantially varied during the first 50 days, which corresponds to a period of high specific conductance and alkalinity values. Correspondingly, anion and cation concentrations were the largest during this early weathering stage and the filter fractions indicated multiple weathering processes, such as particle transport, salt dissolution, and sulfide oxidation. After this early weathering stage, all environmental parameters slowly evolved towards a chemical equilibrium of neutral, oxidizing, and low solute conditions. This evolution was reflected in the decline and stabilization or non-detection of metal(loid) concentrations reflective of a shift to primarily bulk aluminosilicate weathering. Over the course of the experiment, the solute trend of certain elements indicated particular weathering processes— cadmium and nanoparticle transport, selenium and salt dissolution, and arsenic and the oxidation of pyrite. Elements that are found in multiple sources, such as iron, indicated multiple weathering processes that occurred in the early weathering stage and throughout the experiment. The mining of the overburden formations created newly available mineral surfaces and nanoparticles that could release elements into solution that were not expected to be present given historical aquifer water quality for the overburden formations.

Acknowledgments

This project was only possible due to the efforts of many whose time and knowledge was invaluable. Major thanks to the Office of Surface Mining Reclamation and Enforcement for their support and funding, NTEC and Owen Tracy at the Cordero Rojo Mine for their collaboration and outreach, and the Geologic Society of America grant support for this project. I would also like to acknowledge Gaige Swanson and Liam Knudson for their time and work on this project.

I'd also like to thank the faculty in the Earth and Spatial Sciences Department for their time and consideration in courses, research, and beyond. Thank you to Jeff Langman for offering me the opportunity to continue my education and grow to be a better scientist and to Renee Jensen-Hasfurther who goes above and beyond for all students in the Earth and Spatial Sciences Department, much of what we do would be impossible without her.

Dedication

I'd like to dedicate this thesis to those in the Earth and Spatial Sciences Department for their steadfast support and friendship, it's been a great ride. I wish you all the best of luck on the rocky road to graduation and beyond.

Table of Contents

List of Tables

List of Figures

Chapter 1: Introduction

Background

A backfill aquifer is produced from the filling of a mine pit with waste rock (e.g., overburden and interburden materials) and the return of groundwater from infiltrating precipitation or lateral inflow from adjacent aquifers. As water percolates into the waste rock, a reaction front propagates through the aquifer as newly exposed mineral surfaces and small particles (e.g., nanoparticles) are exposed to weathering and transport processes (Jun et al., 2010; Sharma et al., 2015). Progression of the reaction front in weathering waste rock is visible in the temporal evolution of solute release until a new equilibrium of weathering is established (Acero et al., 2009; Blowes & Jambor, 1990; Dosseto et al., 2008; Yoo & Mudd, 2008). The difficulty in understanding the potential water quality of backfill aquifers is not our lack of mineral weathering knowledge, but our lack of understanding of the availability of potential sources contributing to solute release and transport in this modified aquifer matrix. The incomplete source identification for the prediction of solute release has resulted in the exceedance of water quality criteria for backfill aquifers when it was predicted that weathering of the waste rock would not result in groundwater contamination issues (Bartos & Ogle, 2002; Slagle et al., 1985).

Backfill aquifers in the Powder River Basin (Fig. 1.1), the largest coal mining district in the United States, have shown variable water quality and exceedance of water quality criteria for metal(loid) and nonmetal contaminants due to the weathering of waste rock used for landscape restoration. The blasting and transport of the waste rock produce a new aquifer matrix with the generation of new mineral surfaces and nanoparticles that can produce high weathering and solute transport rates (Anderson et al., 2011; Colman, 1981; Dosseto et al., 2008; Drever & Clow, 1995; St-Arnault et al., 2020). A weathering or release rate is the rate at which primary minerals are transformed into secondary minerals or dissolved reaction products, congruently or incongruently, with release of elements/solutes (Colman, 1981). Predicting the release of solutes can be difficult because of coupled and sustained biogeochemical processes, but the identification of potential solute sources and associated reaction rates with the development of an applicable conceptual model is critical for estimating solute release and evaluating future water quality (Futter et al., 2012; M. E.

Malmström et al., 2000; Salmon & Malmström, 2006). A governing physical property of weathering is the available surface area where fine fractions likely undergo the greatest weathering and may be part of localized weathering that releases a substantial portion of the solutes (Banwart et al., 2002; M. Malmström & Banwart, 1997; Stockwell et al., 2006). The generation and transport of nanoparticles, materials with at least one dimension within the nanometer scale (Hochella et al., 2008), can contribute to the solute load through inclusion in dissolved phase (<0.45-µm filtering) and will weather to produce additional solutes during transport (Hochella et al., 2019). Using waste rock from the Cordero Rojo Mine in the Powder River Basin (PRB), a leach column experiment was conducted to discriminate solute sources from newly created mineral surfaces and transportable particles produced with the generation of the waste rock.

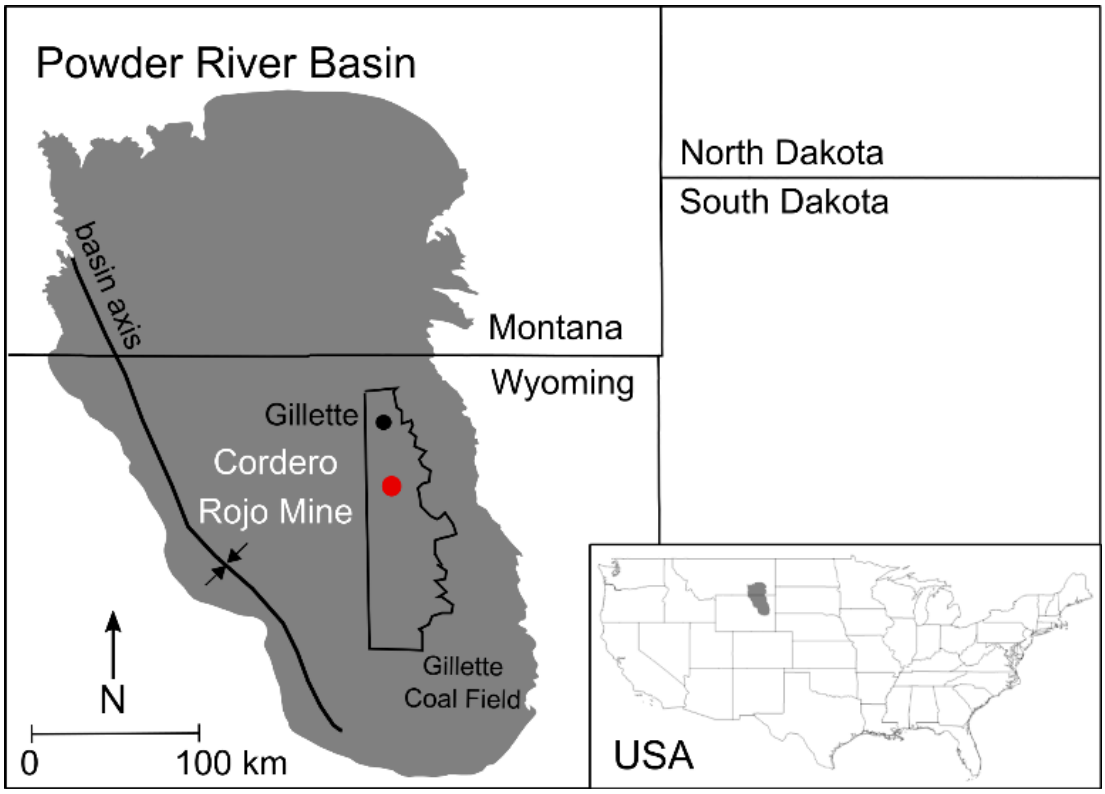

Figure 1.1 Location of the Cordero Rojo Mine in the Powder River Basin of Wyoming, USA (modified layer from the United States Geological Survey, 1999).

Chapter 2: Geology

This chapter covers the geology of the Powder River Basin, the lithology of the main stratigraphic units altered in the Cordero Rojo Mine and the main contaminants found within the altered geologic units.

The PRB (Fig. 1.1) is a north-northwest to south-southeast trending asymmetric syncline that accumulated deposits of marine, alluvial, fluvial, and lacustrine sediments (Dolton et al., 1990). The structural axis is located along the western part of the basin (Fig. 1.1) with the western limb characterized by steeply dipping (~20º) strata and the eastern limb characterized by gently dipping (2–5º) strata, including the coal-bearing rocks (Flores, 2004). The Cordero Rojo Mine extracts its coal from the Wyodak-Anderson coal seam of the Fort Union Formation's Tongue River member that is overlain by upper units of the Paleocene Fort Union and the near-surface Eocene Wasatch formations (Flores & Bader, 1999) (Fig. 2.1). Open pit mining of the coal takes advantage of the near-surface coal deposits along the eastern margin and their gentle westward dip. A typical mining operation consists of a westward-moving open pit, removal of overburden and coal, and the storage of waste rock and subsequent landscape restoration to the east of the active mine site (Fig. 2.2).

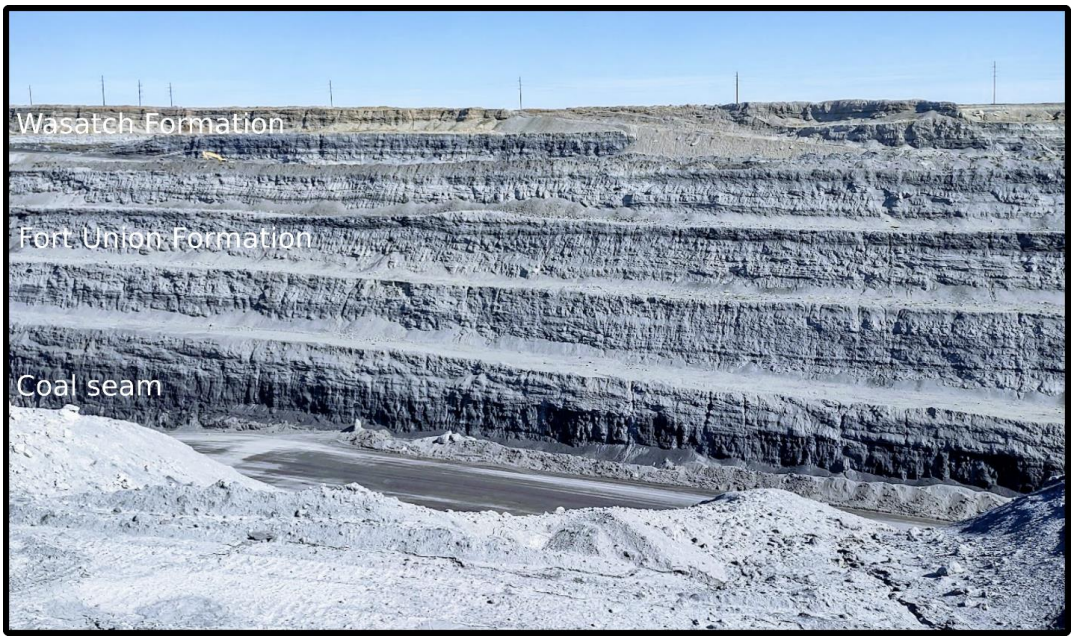

Figure 2.1 Overburden and coal seam at the Cordero Rojo Mine, Powder River Basin, Wyoming, USA.

Figure 2.2 Removal of overburden and waste rock generation during open-pit coal mining at the Cordero Rojo Mine, Powder River Basin, Wyoming, USA.

Waste rock from the Cordero Rojo Mine in the PRB is composed of the Wasatch and Fort Union formations—sequences of interbedded fluvial, lacustrine, and palustrine deposits that compose the overburden (Lorenz & Nadon, 2002; Pocknall, 1987; Yuretich et al., 1984). The Wasatch Formation is composed of sandstones, mudstones, conglomerate lenses, and interbedded limestone and evaporites (Roehler, 1991). The Fort Union Formation is composed of primarily non-sulfidic shales, mudstones, and concretionary sandstones (Hoy et al., 2003; Yuretich et al., 1984) whose paleoenvironments also produced the interbedded low-sulfur coal (Ellis, 2002; McClurg, 1988; Moore, 1991). The PRB coal contains accessory minerals such as arsenic-bearing pyrite [FeS2], cadmium-bearing sphalerite [(Zn,Fe)S], and galena [PbS] (Palmer et al., 1997). Primary contaminants (exceedance of water quality criteria) detected in backfill aquifers of the PRB include arsenic [As], barium [Ba], manganese [Mn], and selenium [Se] (Milligan & Reddy, 2007). Such contamination typically is not found in groundwater that has interacted with the Wasatch and Fort Union formations (Wyoming State Engineer's Office, 1995). Therefore, it was hypothesized that production and disposal of the waste rock have incorporated small coal particles containing higher concentrations of the potential contaminants, exposed previously unavailable forms of the contaminants (e.g., bound salts), and/or produced contaminant-containing nanoparticles that

are being weathered and transported within the backfill aquifers. The goal of this study was to discriminate contaminant sources through the interpretation of solute trends indicative of weathering processes in the waste rock.

Chapter 3: Study Methods

This chapter contains the methodology of all waste rock and leachate testing and the data analyses used in this study.

Waste Rock Characterization

Wasatch and Fort Union waste rock were collected within two weeks of initial excavation from the Cordero Rojo Mine in August of 2021. Sample collection was completed according to the "clean hands" techniques as prescribed for field and laboratory experiments involving trace metals (Environmental Protection Agency, 1996; United States Geological Survey, 2006). Wasatch and Fort Union waste rock were segregated during the mining process, and samples were collected separately per standard practice for sampling aggregates (American Society for Testing and Materials, 2019). The samples were screened in the field to < 6.3 mm to meet the criteria for kinetic columns (American Society for Testing and Materials, 2018a; Lapakko & White, 2000). The 300 kg of screened waste rock (86 kg Wasatch waste rock and 214 kg Fort Union waste rock) was sealed in 0.02 m^3 buckets and transported to the University of Idaho where the waste rock was temporarily stored at 5 °C until dried at 125 °C for 48 hours.

To distinguish potential formation differences in contaminant sources, the Wasatch and Fort Union waste rock were evaluated for element composition (X-ray fluorescence (XRF)), grain-size distribution, weathering resistance (slake durability test), and surface area (Brunauer-Emmett-Teller (BET) analysis). Wasatch and Fort Union waste rock were submitted to the Washington State University GeoAnalytical Laboratory for XRF analysis (Advant'XP+ sequential XRF, fused beads). Grain size distribution and slake durability (American Society for Testing and Materials, 2016) tests were performed at the University of Idaho. Surface area was analyzed by a contract laboratory using a TriStar II Plus High Throughput Surface Area and Porosity Analyzer.

Leachate Experiments

A 20-week, leach column experiment was conducted to evaluate the weathering processes responsible for controlling the release and transport of potential contaminants from the waste rock. Warm-room (20 °C ± 1 °C) and cold-room (5 °C ± 0.5 °C) PVC columns (0.6 m (H) × 0.1 m (W)) were loaded with 0.8 kg of Wasatch waste rock and 3.2

kg Fort Union waste rock to mimic overburden distributions at the Cordero Rojo Mine, which is replicated with backfill aquifer construction. The base of each column contained a two-layer, 2.5-cm thick, non-reactive mesh filter for the retention of the waste rock material while allowing for the passage of particles < 10-µm into the upper portion of the mesh and < 4-µm in the lower portion of the mesh. This dual-layer mesh assisted in retaining bulk solids in the column while minimizing the clogging of the system with the movement of microparticles into the mesh.

The weathering cycle for each leach column consisted of a twice-weekly schedule of the drip introduction of 1-L of deionized water and full saturation of the waste rock for 72 hours followed by a 2-hour drain period and a 6-hour unsaturated period before re-saturation of the column. This is a modification of the standard humidity cell protocol (American Society for Testing and Materials, 2018b) to simulate primarily saturated (e.g., aquifer) conditions and allow for the collection of sufficient water volume for analysis of environmental parameters and solutes. The twice-weekly collection of leachate from each column was analyzed for pH (±0.01 pH), Eh (±0.2 mV), and specific conductance (±0.01 µS/cm) with calibrated Orion 3-Star meters/probes and analysis of anions (0.45-µm filtered) and cations as unfiltered (total), 0.45-µm filtered, and 0.2-µm filtered concentrations. Alkalinity (±0.1 mg/L as $CaCO_3$) was determined by an OrionStarT940 auto titrator using 0.1 N HCl. Unfiltered anion (bromide [Br], chloride [Cl], fluoride [Fl], nitrate-N, nitrite-N [NO_3-N], ortho-phosphate [PO_4], and sulfate [SO_4]) concentrations were determined by ion chromatography (Dionex Aquion Ion Chromatograph). Cation (aluminum [Al], As, Ba, boron [B], Cd, calcium [Ca], chromium [Cr], copper [Cu], iron [Fe], lead [Pb], magnesium [Mg], Mn, molybdenum [Mo], nickel [Ni], potassium [K], Se, sodium [Na], zinc [Zn]) concentrations of unfiltered and filtered samples were determined by inductively coupled plasma optical emission spectrometry (ICP-OES) for larger concentrations (Perkin Elmer Optima 8300 ICP-OES) and inductively coupled plasma mass spectrometry (ICP-MS) for smaller concentrations (Agilent 7800 ICP-MS) at the University of Idaho Analytical Services Laboratory. Duplicate samples were randomly collected during each leachate collection to assess analysis accuracy over the 20-week experiment.

Data Analysis

The goal of the data analysis was the evaluation of the temporal trends, or variability with time, of the environmental conditions and release of solutes for the identification of substantive changes in weathering processes. The temporal trends of the environmental parameters of specific conductance, pH, and alkalinity were smoothed using the moving window average (4-point window) technique to reduce the volatility of the data series and allow for an improved display of the data trends. Values of Eh were not smoothed to preserve reduction-oxidation (redox) conditions that widely varied during the experiment. A principal component analysis (PCA) was used to identify clusters of related metal(loid) solutes for discriminating potential weathering processes in warm and cold conditions and the unfiltered and filter fractions. Solute data sets that were predominantly (> 80 %) below laboratory reporting limits were not included in the PCA.

A Spearman rank correlation analysis of Eh and redox-sensitive elements (As, Fe, Mn, Mo) was performed to identify elements that may reflect the oxidative dissolution of sulfide minerals, such as pyrite, that are present in the Fort Union Formation (Palmer et al., 1997). The Spearman test is a nonparametric measure of rank correlation (statistical dependence between the rankings of two variables) that produces a statistic (ρ) that ranges between +1 (perfect positive relation) and −1 (perfect negative relation). This correlation analysis was performed using only the warm-room unfiltered and filtered values because of substantial non-detection values for these elements in the cold-room leachate. A false discovery rate (q-value) was used in place of a p-value to minimize false negatives. Additionally, the activation energy (E_a, Eq. 1) of the oxidative dissolution of pyrite was calculated to evaluate temporal changes in pyrite weathering that may indicate inhibition of sulfide weathering because of precipitate formation (Fan et al., 2022, p. 20122). Arsenic was selected for the calculation of the activation energy because of its strong correlation with Eh and the presence of Fe and sulfur [S] in other mineral sources found in the waste rock (Kolker et al., 2002). The Arrhenius equation using a single temperature and rate constant (Eq. 1) was used to calculate E_a instead of the typical two-temperature/two-rate constant method because cold-room As concentrations decreased below detection levels during the experiment. The one temperature/rate constant method

employs the geometric solution or slope (line of best fit) of the ln k-to-time relation for estimating E_a:

$$\ln(k) = \ln(\mathrm{A}) - \left(\frac{\mathrm{Ea}}{\mathrm{RT}}\right) \qquad \text{Eq. 3.1}$$

where E_a is the activation energy ($J \cdot mol^{-1}$), R is the universal gas constant (8.314×10^{-3} $J \cdot mol^{-1} \cdot K^{-1}$), A is a pre-exponential factor (s^{-1}), and T is the temperature (K) at the respective times of the observed rate constants (k in $mol \cdot m^{-2} \cdot s^{-1}$).

Chapter 4: Results and Discussion

This chapter covers the results of waste rock chemical and physical characterization, leachate testing results, and data analysis of all reported data. This includes the discussion of weathering processes and characterization of weathering dynamics within the mine waste rock for representative elemental constituents.

Waste Rock Characterization

Large concentrations of Al and silicon [Si] were present in the Wasatch and Fort Union waste rock reflective of the dominant aluminosilicate minerals that compose these fluvial and lacustrine deposits (Dolton et al., 1990; Roehler, 1987) (Fig. 4). Larger accumulations of redox-sensitive elements of Fe and Mn were present in the Fort Union waste rock, which are indicative of the low-energy paleoenvironments associated with certain units of the Fort Union Formation (Ayers, 1986; Hagmaier, 1971). The slake durability tests indicated stronger rock (93 % durability index) from the Wasatch Formation compared to the durability index of 89 % for rock from the Fort Union Formation. Such results align with the presence of substantial sandstone in the Wasatch Formation (Roehler, 1991) compared to the higher content of shales and mudstones in the Fort Union Formation (Ayers, 1986). Correspondingly, the grain size distribution analysis indicated a greater fraction of clay-sized particles (7.6 %) present in the Fort Union waste rock. The greater presence of smaller particles in the Fort Union waste rock also translated to a greater surface area of 14.2 m^2/g compared to the 5.1 m^2/g for the Wasatch sample.

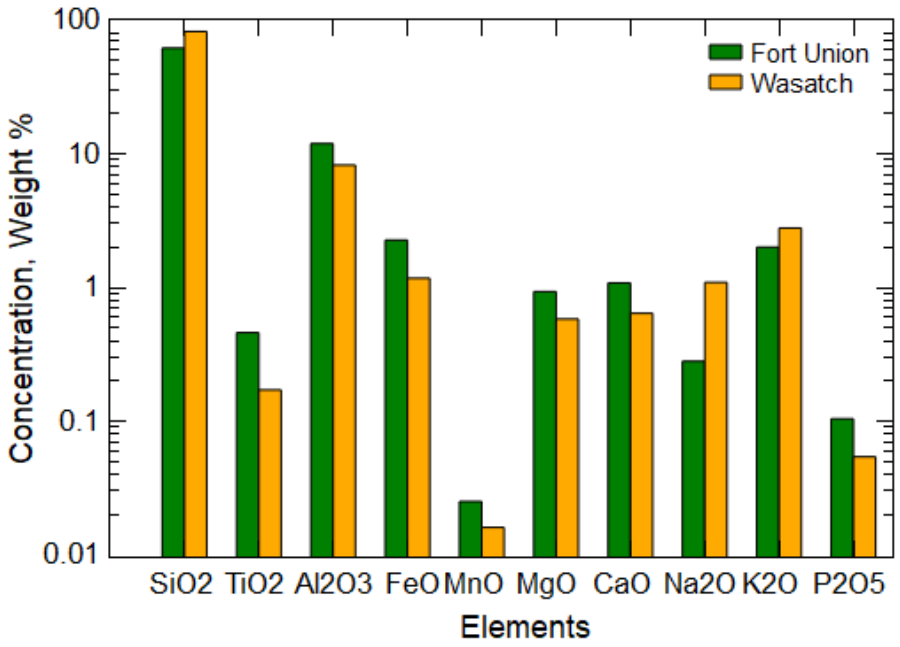

Figure 4.1 Element composition of the Fort Union and Wasatch waste rock from the Cordero Rojo Mine.

Leachate Environmental Conditions

The environmental conditions for warm- and cold-room leachate indicated high variability during the first 50+ days of the experiment (Fig. 5). Eh fluctuated between positive values (maximum of 142 mV for warm-room leachate and 154 mV for cold-room leachate) and negative values (minimum of −113 mV for the warm-room leachate and −118 mV for the cold-room leachate) indicating alternating oxidizing and reducing conditions with the greatest variability during the first 45 days. Specific conductance ranged from 6,410 µS/cm to 315 µS/cm for the warm-room leachate and 6,350 µS/cm to 271 µS/cm for cold-room leachate, and the specific conductance of leachate from both columns decreased sharply during the first 40 days of the experiment (Fig. 5b). Values of pH remained near neutral for the entire experiment, ranging from 6.05 to 7.03 for the warm-room leachate and 6.47 to 7.04 for the cold-room leachate (Fig. 5c) but indicated a greater temperature difference in pH values during the first 55 days. Alkalinity ranged from 550 mg/L to 148.3 mg/L for the warm-room leachate and 613 mg/L to 139 mg/L for the cold-room leachate (Fig. 5d) with a sharp decline during the first 20 days and a slower decrease from Day 20 to Day 70.

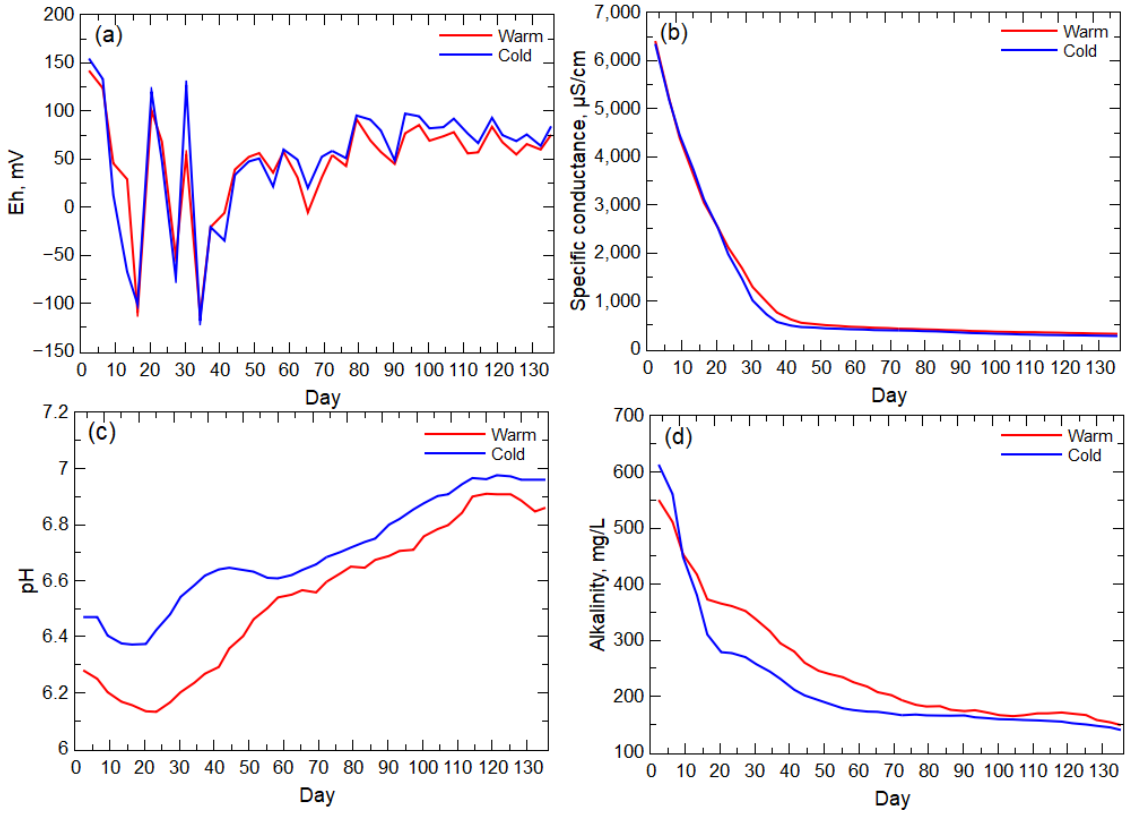

Figure 4.2 (a) Eh, (b) specific conductance, (c) pH, and (d) alkalinity for leachate from the warm- and cold-rooms. All trendlines have been smoothed using the moving window average (4-point window) technique except for Eh.

The high solute release period (early weathering stage) indicated by the specific conductance trends likely is a result of the flushing of nano- to micro-particles and the influence of fast reaction weathering, such as sulfide oxidation (Harrison et al., 2017; St-Arnault et al., 2020), when the largest surface area of these minerals was available. This early weathering stage (Day 3 to Day 31, specific conductance >1000 µS/cm) also corresponds to sharp decreases and increases in Eh values and the period of maximum pH difference indicative of oxygen-consuming and acid-generating reactions, such as the oxidative dissolution of pyrite (Nordstrom et al., 2011). The lessening of the temperature effect on pH by Day 55 corresponds to the stabilization of positive Eh values and the slowing of the decrease in the specific conductance trend (past the inflection point), which indicate a shift to weathering of less reactive minerals (e.g., aluminosilicates) and loss (consumption) of the more reactive sulfide minerals. Alkalinity values in the warm- and cold-room leachate remained elevated past this early weathering stage indicative of the relatively slower reactivity of available carbonate minerals (Colman, 1981; Yoo &

Mudd, 2008), which have been identified in the Wasatch Formation (Palmer et al., 2001; Roehler, 1991).

Weathering Processes and Solute Trends

The first component (PC1, Table 1) of the PCA indicated an association (covariance of 0.14) of the major cations (Ca, Mg, and K) along with Mn, Ni, and Zn that is consistent in the total and filtered concentrations in warm- and cold-room conditions (Table 1, blue bold values). This association of the major ions in unfiltered and filtered samples indicates primarily bulk aluminosilicate and carbonate weathering throughout the experiment. The inclusion of Mn and Zn in this associated group likely reflects the presence of Mn and Zn-bearing carbonate species that have been identified in the Powder River Basin waste rock formations (Palmer et al., 2001). Additionally, Ni is likely associated in a clay source (R. Finkelman, 1987; R. B. Finkelman et al., 2018a; Palmer et al., 2001). The association of the redox-sensitive Mn with elements released from manganese-oxide minerals found in the Wasatch Formation (Sharp et al. 1964) is supported by the lack of correlation (Spearman ρ of -0.04 to -0.03, q-value of 0.84) between Eh and Mn concentrations (unfiltered or filtered), where a correlation would be expected if the Mn was being released with sulfide oxidation. The second component (PC2, Table 1) of the PCA indicated a correlation of As and filtered Fe concentrations likely because of their association in sulfide minerals (e.g., As-bearing pyrite) that can be found in the Wyodak-Anderson coal (Ellis, 2002; R. B. Finkelman et al., 2018b). The second component also indicated an opposing correlation of Mo (positive) and Fe and As (negative) in the warm-room leachate (lack of detectable concentrations in the cold-room leachate), which may be indicative of the presence of Mo in the coal (Frascoli & Hudson-Edwards, 2018) but has a different mineral source than Fe and As. The association of Mo in PC2 is likely derived from a silicate or organic source (Palmer et al., 2001), supported by the strong, positive correlation (Spearman's ρ of 0.58 to 0.55, q-value of 0.0009) between Mo and Eh. The oxidation of an organic source may lead to the release of Mo in organic sources (Horan, 2018).

Table 4.1 The covariance matrix of the principal component analysis for warm- and cold-room solute concentrations for each concentration fraction (total (unfiltered), 0.45-µm filtered, and 0.2-µm filtered). Two principal components (PC1 and PC2) are shown along with noted associations through bold and colored fonts.

Element		Warm			Cold		
		Total	**0.45-µm**	**0.2-µm**	**Total**	**0.45-µm**	**0.2-µm**
As	PC1	0.02	0.03	0.03	0.09	0.13	0.13
	PC2	**-0.29**	**-0.26**	**-0.27**	-0.09	0.12	0.13
Ba	PC1	-0.13	-0.13	-0.13	-0.12	-0.13	-0.13
	PC2	0.09	0.09	0.09	0.14	0.14	0.14
B	PC1	0.11	0.14	0.14	0.09	0.14	0.14
	PC2	-0.05	0.01	0.01	0.06	-0.05	-0.05
Ca	PC1	**0.15**	**0.15**	**0.15**	**0.14**	**0.14**	**0.14**
	PC2	0.01	0.01	0.01	-0.03	-0.02	-0.02
Fe	PC1	0.11	0.06	0.07	0.03	-0.06	-0.06
	PC2	**-0.12**	**-0.27**	**-0.26**	0.14	-0.01	-0.01
Mg	PC1	**0.14**	**0.14**	**0.14**	**0.14**	**0.14**	**0.14**
	PC2	0.07	0.07	0.07	0.05	0.05	0.05
Mn	PC1	**0.14**	**0.14**	**0.14**	**0.14**	**0.14**	**0.14**
	PC2	-0.07	-0.07	-0.06	-0.04	-0.01	-0.01
Mo	PC1	-0.02	-0.02	-0.01	0.03	0.03	0.03
	PC2	0.26	0.25	0.27	0.23	0.26	0.26
Ni	PC1	**0.14**	**0.14**	**0.14**	**0.14**	**0.14**	**0.14**
	PC2	0.04	0.05	0.05	0.07	0.08	0.08
K	PC1	**0.14**	**0.14**	**0.14**	**0.14**	**0.14**	**0.14**
	PC2	0.04	0.05	0.05	0.03	0.03	0.03
Zn	PC1	**0.14**	**0.14**	**0.14**	**0.14**	**0.14**	**0.14**
	PC2	0.06	0.04	0.06	0.05	0.04	0.04

Salt Dissolution and Nanoparticle Flushing

The PCA did not include elements such as Cd and Se that were only detectable in the leachate during the first two weeks of the experiment (Fig. 4.3a,b). These elements have an association with sulfide minerals in the PRB coal (Bao et al., 2022; Kolker et al., 2002; Yudovich & Ketris, 2006), but their concentration trends did not mimic a release with the oxidative dissolution of pyrite that is visible with the As concentrations (Fig. 4.3c). In the waste rock formations, Se can be found in the coal, coal-associated pyrite, water-leachable salts, and as sorbed particles (e.g., selenite [SeO_3]) (Yudovich & Ketris, 2006). Dreher & Finkelman (1992) indicated that Se salts from past oxidation of pyrite may be the primary source of Se in the overburden; although they found seven different

forms of Se with no discrimination between Wasatch and Fort Union formations. The quick release of Se and lack of difference within filter fraction concentrations and between temperature conditions are indicative of a fast-dissolving salt and/or desorption and oxidation of Se particles, such as selenite. The incorporation of Se into gypsum [$CaSO_4$] can occur with the oxidation of pyrite/coal and the substitution of Se for S in gypsum (Stillings, 2017; H. Wang et al., 2021). Such processes are partially responsible for the significant presence of gypsum in Powder River Basin sedimentary formations (Healy et al., 2008; Lee, 1980; Rice et al., 2008; See et al., 1995). Se-bearing salts can readily dissolve, but the dissolution of the salts may not contribute substantial soluble Se species (e.g., selenate [SeO_4^{2-}]) if selenite is produced given the preference of selenite to readily sorb to sediments (Elrashidi et al., 1987; Paydary et al., 2021; Torres et al., 2011). The Se release from the leach column appears to be influenced both by particle release (early and large concentrations) with contributions from Se salt dissolution that is more visible in the second week when the warm-room leachate indicated higher concentrations of Se.

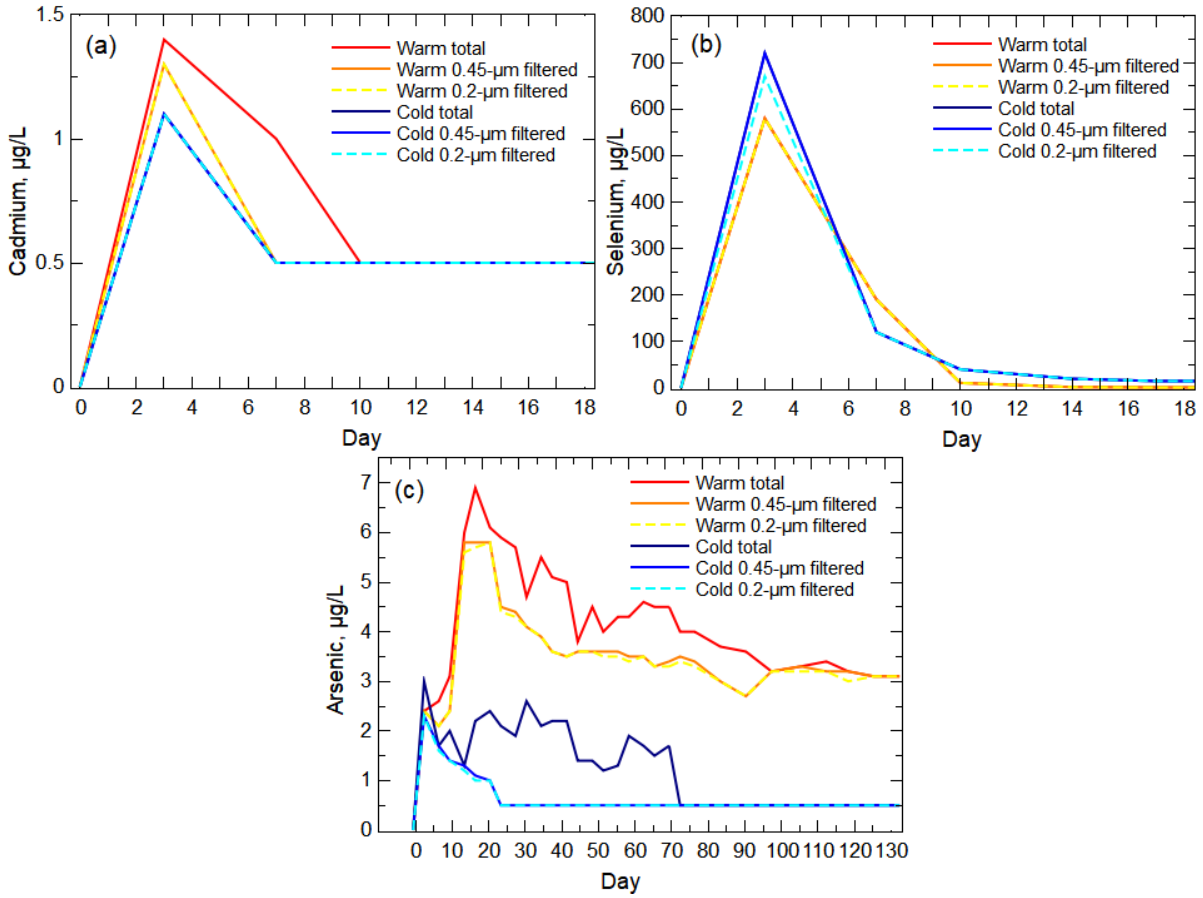

Figure 4.3 Unfiltered (total) and filtered concentrations in the warm-room and cold-room leachate for (a) cadmium and (b) selenium during the first 18 days of the experiment and (c) arsenic during the entire length of the experiment. All non-detect values were set to 0.5 µg/L, which is half the reporting limit for each of the analytes.

The Cd trend in the leachate indicates an early concentration peak that quickly decreased below reporting limits after Day 3 for all filtered warm- and cold-room results, and after Day 7 for total (unfiltered) warm-room leachate (Fig. 4.3a). Cadmium has not been documented as a salt byproduct from the oxidation of sulfide minerals in the Fort Union Formation, but Cd is associated with sphalerite [(Fe,Zn)S] found in PRB coal (R. B. Finkelman et al., 2018a). Given the presence of Se salts from the oxidation of pyrite, it can be assumed that Cd was similarly released with sphalerite oxidation and deposited in the overburden formations. The introduction of leach water to the waste rock would not have a similar mobilizing effect on Cd compared to Se if both elements are contained in readily dissolvable salts since Cd is less soluble than Se (Stoeppler, 1992). This lower solubility of Cd is reflected in the much lower concentrations of Cd released from the

waste rock compared to Se (Fig. 4.3) even though there are equivalent amounts of Cd and Se in the Wyodak-Anderson coal seam (Brownfield et al., 2005). With the lower solubility of Cd, it is assumed that the release of Cd from the waste rock early in the experiment is because of the transport of Cd-bearing particles, primarily nanoparticles (X. Li et al., 2022). Not all of the Cd was present in nanoparticles given the greater release of Cd in the unfiltered warm-room leachate, which indicated a more torturous path of the release of larger particles being transported from the waste rock. Comparison of the pre-experiment Wasatch and Fort Union samples to post-experiment waste rock from the warm-room, leach column indicated the loss of the smallest grains (< 0.07 mm) from the Fort Union sample pre-experiment waste rock indicative of the loss (e.g., transport, weathering) of small particles (Fig. 4.4).

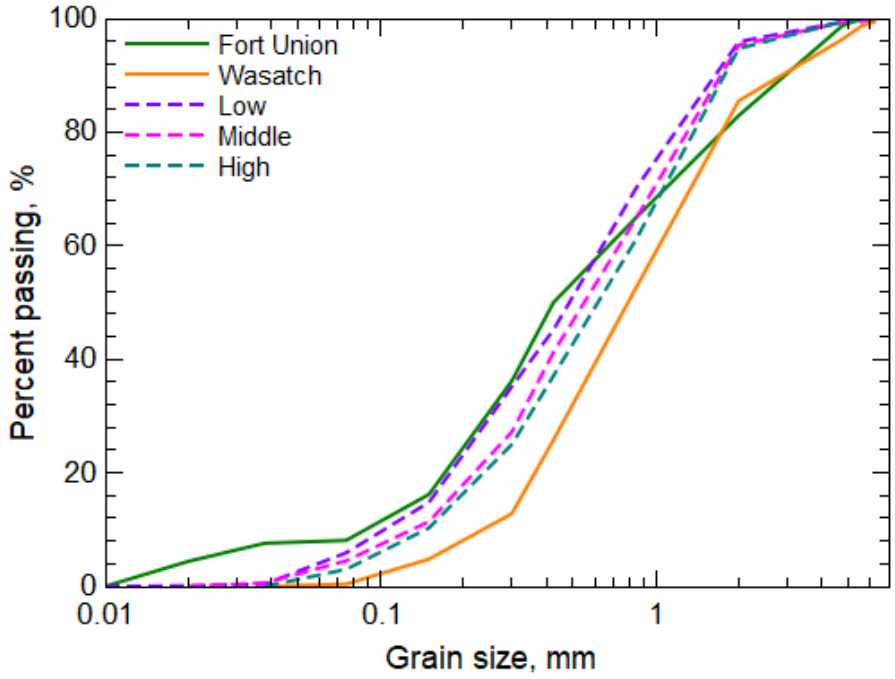

Figure 4.4 Grain size analysis of waste rock from the pre-experiment Fort Union and Wasatch samples and post-experimental waste rock sampled at three locations within the warm-room, leach column (low, middle, and high).

Sulfide Oxidation Reactions

Arsenic concentrations were largest in warm-room and cold-room leachate during the early weathering stage when Eh varied between positive and negative values (Fig. 4.2c) reflective of the likely consumption of oxygen with sulfide mineral weathering. The correlation analysis also indicated a strong to moderate negative correlation (Spearman's ρ of -0.56 to -0.29, q-value of 0.0009 to 0.1) between As and Eh. The majority of the As

released in the warm-room leachate was present in the 0.2-μm filtered samples indicating ion release and/or small nanoparticles. The unfiltered leachate from both temperature conditions indicated the possible As release in microparticles being transported from the columns. The release of an element such as As with pyrite weathering typically would result in an initial peak concentration because of the dissolution of an outer layer (rim or coating) followed by a moderated release according to the mass-to-volume ratio of the available mineral source (Acero et al., 2007). The primary loss of As from the waste rock is in the filtered fractions with a trend that peaks near Day 17 followed by a moderate decrease. The post-peak release of As is indicative of weathering of the As-bearing pyrite contained in the PRB coal that was incorporated into the waste rock. Such a trend follows the expected element release with the oxidative dissolution of pyrite (Williamson & Rimstidt, 1994). Calculation of the effective activation energy of pyrite weathering (Fig. 4.5) for weathering and transport presents a typical energy trend of an initial energy barrier (oxidation of the mineral surface), an early drop in energy barrier as the sulfide surface degrades, and a slow increase in the necessary energy for oxidation of the remaining sulfide mineral. This trend represents the oxidation of the unreacted sulfide surface (shrinking core model) that becomes controlled by the inward diffusion of oxygen given the pore-blocking effect of Fe and S precipitates on the unreacted sulfide surface (Hu et al., 2006, p. 200). This oxygen diffusion effect is more pronounced in neutral conditions where Fe is not solubilized and can form substantial Fe (oxyhydr)oxides with the eventual loss of the S intermediaries (Langman et al., 2015; Wunderly et al., 1996). The effective activation energy trend aligns with the evolution of activation energy necessary for the different bonding arrangements where the initial dissociation of oxygen at the sulfide surface required an activation energy of 22.6 kJ/mol (Dos Santos et al., 2016) (compared to our calculated 18.2 kJ/mol) followed by lower energy requirements with degradation of the mineral structure.

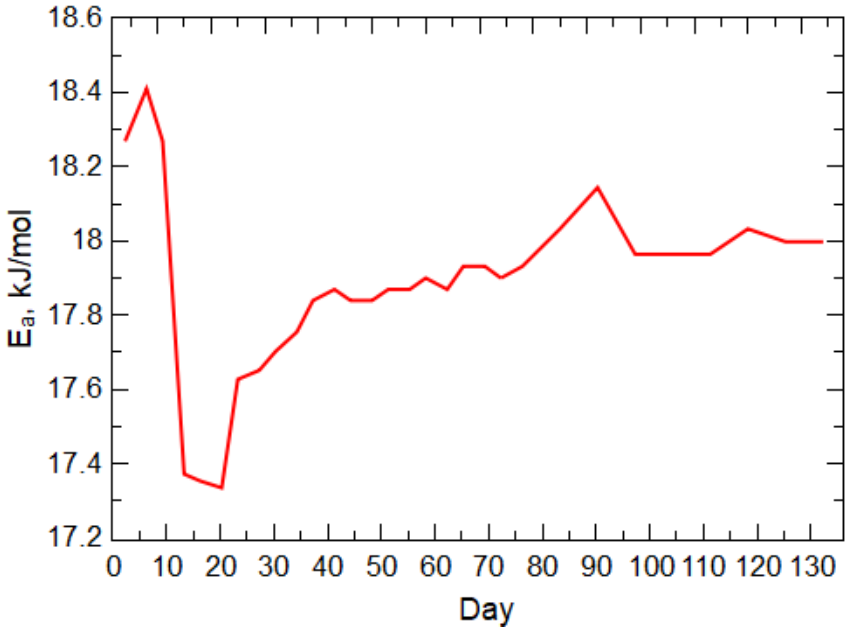

Figure 4.5 Activation energy (Ea) of pyrite weathering derived from warm-room, leach column arsenic concentrations during the 20-week experiment.

Bulk Weathering

With the identification of salt dissolution, particle transport, and pyrite oxidation contributing to the high solute release period, an additional weathering process is necessary to explain the large concentrations in all solutes during the early weathering stage and the following period of higher alkalinity (Fig. 4.2). Transport of other particle types and weathering of the bulk aluminosilicate and carbonate minerals likely explains the remaining contributions to the high solute and high alkalinity periods prior to the waste rock equilibrating to the low solute weathering period (post-Day 70). Carbonates typically weather at a higher rate compared to aluminosilicates (Lehmann et al., 2022), which may explain the higher Ca concentrations compared to K (Fig. 4.6) even though there is greater K present in the Wasatch and Fort Union waste rock (Fig. 4.1). Carbonate weathering likely is responsible for the pH moderation during pyrite oxidation and increase during the experiment (Fig. 4.2), as well as the longer period of high alkalinity compared to the specific conductance period. The large, early concentrations in each of these element's concentration trends suggest release of Ca- and K-bearing nanoparticles (Hochella et al., 2019), desorption (exchangeable ions) from larger particles (Agbenin & van Raij, 1999), or loss from roughened surfaces (White et al., 1996) followed by a

typical slow release of these elements with bulk silicate weathering (Skorina & Allanore, 2015; Sparks, 1991). Warm-room leachate shows higher initial concentrations than cold-room leachate for both K and Ca, which is likely the result of temperature and pH controls on desorption and mineral degradation (Brazier et al., 2019; Dreybrodt et al., 1996; Gaillardet et al., 2019; Lasaga, 1984; W. Li et al., 2021; White & Brantley, 1995).

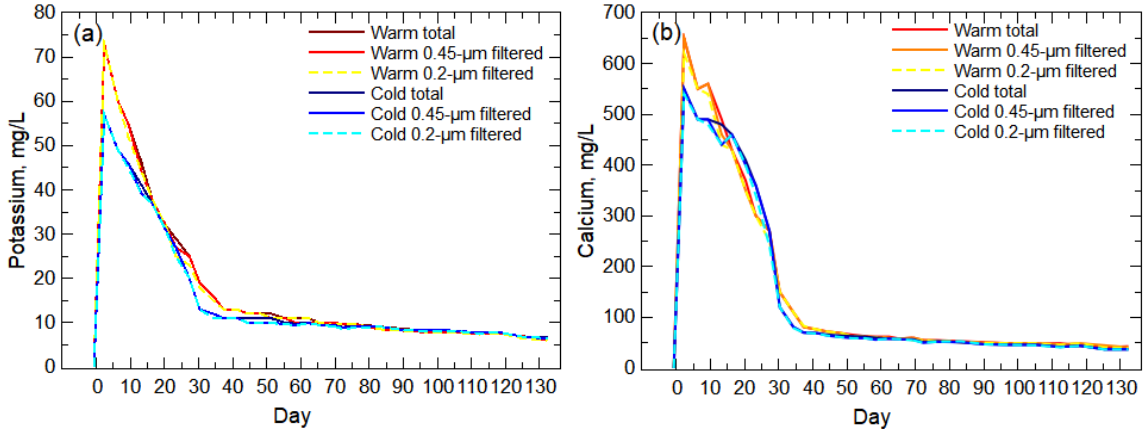

Figure 4.6 Potassium (a) and calcium (b) unfiltered (total) and filtered concentrations for the warm-room and cold-room leachate during the 20-week leach column experiment.

Complex Weathering

Iron concentrations for warm- and cold-room leachate indicated multiple weathering processes causing the release of Fe over the course of the experiment (Fig. 10). Iron content in the Wasatch and Fort Union waste rock is substantial (Fig. 4) and likely has multiple mineral sources, including sulfides (pyrite) and aluminosilicates (feldspars and associated clays) along with sorbed Fe (oxyhydr)oxides. The relation of Fe and Eh was a moderate to weak, negative correlation (Spearman's ρ of −0.31 for the filtered concentrations (q-value of 0.01) and −0.11 for the unfiltered concentrations (q-value of 0.7)), likely as a result of the variety of Fe sources and solubility controls on Fe. Given the low solubility of Fe^{3+} in oxidizing and near-neutral pH (Hem & Cropper, 1962; Schwertmann, 1991), Fe likely was released from the waste rock as desorbed Fe (oxyhydr)oxides particles early in the experiment, which accounts for the large total Fe concentration peaks at Day 3. The potential for mobile Fe forms is a complex interaction of environmental conditions and solute composition and concentrations that commonly results in the formation of nanoscale to colloidal Fe particles (Davison, 1993; Gaffney et al., 2008; Hassellöv & von der Kammer, 2008; Liang & Morgan, 1990; Perret et al.,

2000). The much larger concentration of Fe in the warm-room leachate during the initial peak contained substantially higher total Fe concentrations during this first week of the experiment indicative of the effect of pH and temperature on Fe-particle desorption and transport (Hatje et al., 2003; Possemiers et al., 2016; Weber et al., 2010). After the initial peak of Fe, there is a substantial release of Fe from the warm-room leachate with oxidation of the pyrite that is limited under colder temperatures (Sun et al., 2015). As Fe forms are mobilized and removed from the waste rock along with reduction of available sulfide surfaces, Fe starts to weather at a consistent and lower release rate at approximately Day 65 (Fig. 10) similar to the trends of Ca and K (Fig. 9). This Fe trend potentially is the result and the release of Fe (oxyhydr)oxide particles with weathering of the bulk solids and continued desorption and particle aggregation/de-aggregation with transport (Journet et al., 2008; Z. Wang et al., 2018).

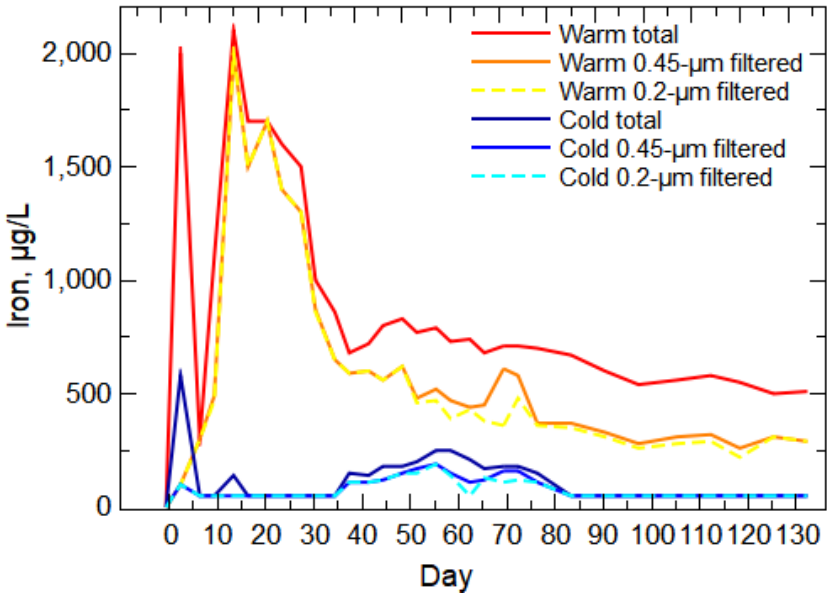

Figure 4.7 Iron unfiltered (total) and filtered concentrations for warm-room and cold-room leachate during the 20-week leach column experiment. Non-detect values were set to half the reporting limit (50 µg/L).

Chapter 5: Conclusions

The construction of backfill aquifers during restoration of mine sites may cause water quality impacts during the early stages of groundwater infiltration and weathering of waste rock because of new solute sources, such as freshly exposed mineral surfaces and the generation of transportable particles. Monitoring of groundwater in open-pit coal mine backfill aquifers in Powder River Basin, Wyoming, has indicated variable water quality impacts that were not expected given groundwater quality in aquifers contained in the overburden formations. A 20-week leach column experiment was conducted to characterize weathering sources and processes using waste rock from the Cordero Rojo Mine in the Powder River Basin. Analysis of the Eh, pH, specific conductance, and alkalinity of the leachate collected from warm-room and cold-room columns indicated an early weathering stage during the first 50 days of the experiment that produced large solute concentrations. Additionally, relatively high alkalinity values indicated a transitional stage weathering period followed by a low solute period as the waste rock began to weather in an apparent equilibrium state. Multiple weathering processes were identified from solute release—nano- and micro-particle flushing, salt dissolution, oxidative dissolution of sulfide minerals, carbonate weathering, and the weathering of the bulk aluminosilicate matrix. Certain elements indicated one or two primary weathering processes that released the element into solution—cadmium from particle flushing, selenium from salt dissolution and particle flushing, arsenic from pyrite oxidation, calcium from particle flushing and carbonate dissolution, and potassium from particle flushing and aluminosilicate weathering. Multiple mineral sources for an element such as iron produced complex weathering trends with concurrent or sequential weathering processes occurring throughout the duration of the experiment. The mining and landscape restoration process produces newly exposed mineral surfaces and fine particles that may be weathered and transported in groundwater, creating water quality issues not expected given historical aquifer water quality in the unaltered regional geology.

Work Cited

Acero, P., Ayora, C., Carrera, J., Saaltink, M. W., & Olivella, S. (2009). Multiphase flow and reactive transport model in vadose tailings. *Applied Geochemistry*, *24*(7), 1238–1250. https://doi.org/10.1016/j.apgeochem.2009.03.008

Acero, P., Cama, J., & Ayora, C. (2007). Sphalerite dissolution kinetics in acidic environment. *Applied Geochemistry*, *22*(9), 1872–1883. https://doi.org/10.1016/j.apgeochem.2007.03.051

Agbenin, J. O., & van Raij, B. (1999). Rate processes of calcium, magnesium and potassium desorption from variable-charge soils by mixed ion-exchange resins. *Geoderma*, *93*(1), 141–157. https://doi.org/10.1016/S0016-7061(99)00049-X

American Society for Testing and Materials. (2016). *Standard Test Method for Slake Durability of Shales and Similar Weak Rocks* (ASTM No. D4644-87). American Society for Testing Materials. https://doi.org/10.1520/D4644-16

American Society for Testing and Materials. (2018a). *Standard Practice for Reducing Samples of Aggregate to Testing Size* (ASTM C702/C702M-18). ASTM International. https://doi.org/10.1520/C0702_C0702M-18

American Society for Testing and Materials. (2018b). *Standard Test Method for Laboratory Weathering of Solid Materials Using a Humidity Cell* (ASTM No. D5744-18). ASTM International. https://doi.org/10.1520/D5744-18

American Society for Testing and Materials. (2019). *Standard Practice for Sampling Aggregates* (ASTM D75/D75M-19). ASTM International. https://doi.org/10.1520/D0075_D0075M-19

Anderson, S. P., Anderson, R. S., Hinckley, E.-L. S., Kelly, P., & Blum, A. (2011). Exploring weathering and regolith transport controls on Critical Zone development with models and natural experiments. *Applied Geochemistry*, *26*, S3–S5. https://doi.org/10.1016/j.apgeochem.2011.03.014

Ayers, J. (1986). Lacustrine and fluvial-deltaic depositional systems, Fort Union Formation (Paleocene), Powder River basin, Wyoming and Montana. *Am. Assoc. Pet. Geol., Bull.; (United States)*, *70:11*. https://www.osti.gov/biblio/7152938

Banwart, S. A., Evans, K. A., & Croxford, S. (2002). Predicting mineral weathering rates at field scale for mine water risk assessment. *Geological Society, London, Special Publications*, *198*(1), 137–157. https://doi.org/10.1144/GSL.SP.2002.198.01.10

Bao, Z., Al, T., Bain, J., Shrimpton, H. K., Finfrock, Y. Z., Ptacek, C. J., & Blowes, D. W. (2022). Sphalerite weathering and controls on Zn and Cd migration in mine waste rock: An integrated study from the molecular scale to the field scale. *Geochimica et Cosmochimica Acta*, *318*, 1–18. https://doi.org/10.1016/j.gca.2021.11.007

Bartos, T., & Ogle, K. M. (2002). *Water Quality and Environmental Isotopic Analyses of Ground-Water Samples Collected from the Wasatch and Fort Union Formations in Areas of Coalbed Methane Development—Implications to Recharge and Ground-Water Flow, Eastern Powder River Basin, Wyoming* (Water Resources Investigations Report No. 02–4045). U.S. Geological Survey. https://doi.org/10.3133/wri024045

Blowes, D. W., & Jambor, J. L. (1990). The pore-water geochemistry and the mineralogy of the vadose zone of sulfide tailings, Waite Amulet, Quebec, Canada. *Applied Geochemistry*, *5*(3), 327–346. https://doi.org/10.1016/0883-2927(90)90008-S

Brazier, J.-M., Schmitt, A.-D., Gangloff, S., Pelt, E., Chabaux, F., & Tertre, E. (2019). Calcium isotopic fractionation during adsorption onto and desorption from soil phyllosilicates (kaolinite, montmorillonite and muscovite). *Geochimica et Cosmochimica Acta*, *250*, 324–347. https://doi.org/10.1016/j.gca.2019.02.017

Brownfield, M., Cathcart, J. D., Affolter, R. H., Brownfield, I. K., Rice, C. A., O'Connor, J. T., Zielinski, R. A., Bullock, J. H., Hower, J. C., & Meeker, G. P. (2005). *Characterization and Modes of Occurrence of Elements in Feed Coal and Coal Combustion Products from a Power Plant Utilizing Low-Sulfur Coal from the Powder River Basin, Wyoming* (Scientific Investigations No. 2004–5271; p. 36). U.S. Geological Survey. http://pubs.usgs.gov/sir/2004/5271/

Colman, S. M. (1981). Rock-Weathering Rates as Functions of Time. *Quaternary Research*, *15*(3), 250–264. https://doi.org/10.1016/0033-5894(81)90029-6

Davison, W. (1993). Iron and manganese in lakes. *Earth-Science Reviews*, *34*(2), 119–163. https://doi.org/10.1016/0012-8252(93)90029-7

Dolton, G. L., Fox, J. E., & Clayton, J. L. (1990). *Petroleum geology of the Powder River basin, Wyoming and Montana* (Open-File No. 88-450-P). U.S. Geological Survey. https://doi.org/10.3133/ofr88450P

Dos Santos, E. C., de Mendonça Silva, J. C., & Duarte, H. A. (2016). Pyrite Oxidation Mechanism by Oxygen in Aqueous Medium. *The Journal of Physical Chemistry C*, *120*(5), 2760–2768. https://doi.org/10.1021/acs.jpcc.5b10949

Dosseto, A., Turner, S. P., & Chappell, J. (2008). The evolution of weathering profiles through time: New insights from uranium-series isotopes. *Earth and Planetary Science Letters*, *274*(3), 359–371. https://doi.org/10.1016/j.epsl.2008.07.050

Dreher, G. B., & Finkelman, R. B. (1992). Selenium mobilization in a surface coal mine, Powder River Basin, Wyoming, U.S.A. *Environmental Geology and Water Sciences*, *19*(3), 155–167. https://doi.org/10.1007/BF01704083

Drever, J. I., & Clow, D. W. (1995). Weathering rates in catchments. In *Chemical Weathering Rates of Silicate Minerals* (Vol. 31, pp. 463–483). De Gruyter. https://doi.org/10.1515/9781501509650-012

Dreybrodt, W., Lauckner, J., Zaihua, L., Svensson, U., & Buhmann, D. (1996). The kinetics of the reaction CO2 + H2O → H+ + HCO3− as one of the rate limiting steps for the dissolution of calcite in the system H2O□CO2□CaCO3. *Geochimica et Cosmochimica Acta*, *60*(18), 3375–3381. https://doi.org/10.1016/0016-7037(96)00181-0

Ellis, M. S. (2002). *Quality of economically extractable coal beds in the Gillette coal field as compared with other Tertiary coal beds in the Powder River basin, Wyoming and Montana* (USGS Numbered Series No. 2002–174; Open-File Report). U.S. Geological Survey. https://doi.org/10.3133/ofr02174

Elrashidi, M. A., Adriano, D. C., Workman, S. M., & Lindsay, W. L. (1987). Chemical Equilibria of Selenium in Soils: A Theoretical Development. *Soil Science*, *144*(2), 141–152.

Environmental Protection Agency. (1996). *Sampling Ambient Water for Trace Metals at EPA Water Quality Criteria Levels Method 1669*.

Fan, R., Qian, G., Li, Y., Short, M. D., Schumann, R. C., Chen, M., Smart, R. S. C., & Gerson, A. R. (2022). Evolution of pyrite oxidation from a 10-year kinetic leach study: Implications for secondary mineralisation in acid mine drainage control. *Chemical Geology*, *588*, 120653. https://doi.org/10.1016/j.chemgeo.2021.120653

Finkelman, R. (1987). The Inorganic Geochemistry of Coal: A Scanning Electron Microscopy View. *Scanning Microscopy*, *2*(1), 97–105.

Finkelman, R. B., Palmer, C. A., & Wang, P. (2018a). Quantification of the modes of occurrence of 42 elements in coal. *International Journal of Coal Geology*, *185*, 138–160. https://doi.org/10.1016/j.coal.2017.09.005

Finkelman, R. B., Palmer, C. A., & Wang, P. (2018b). Quantification of the modes of occurrence of 42 elements in coal. *International Journal of Coal Geology*, *185*, 138–160. https://doi.org/10.1016/j.coal.2017.09.005

Flores, R. M. (2004). *Total Petroleum System and Assessment of Coalbed Gas in the Powder River Basin Province, Wyoming and Montana*. USGS. https://pubs.usgs.gov/dds/dds-069/dds-069-c/REPORTS/Chapter_2.pdf

Flores, R. M., & Bader, L. R. (1999). *Fort Union Coal in the Powder River Basin, Wyoming and Montana: A Synthesis* (No. 1625-A; Resource Assessment of Selected Teriary Coal Beds and Zones in the Northern Rocky Mountains and Great Plains Region). U.S. Geologic Survey. https://pubs.usgs.gov/pp/p1625a/Chapters/PS.pdf

Frascoli, F., & Hudson-Edwards, K. A. (2018). Geochemistry, Mineralogy and Microbiology of Molybdenum in Mining-Affected Environments. *Minerals*, *8*(2), Article 2. https://doi.org/10.3390/min8020042

Futter, M. N., Klaminder, J., Lucas, R. W., Laudon, H., & Köhler, S. J. (2012). Uncertainty in silicate mineral weathering rate estimates: Source partitioning and policy implications. *Environmental Research Letters*, *7*(2), 024025. https://doi.org/10.1088/1748-9326/7/2/024025

Gaffney, J. W., White, K. N., & Boult, S. (2008). Oxidation State and Size of Fe Controlled by Organic Matter in Natural Waters. *Environmental Science & Technology*, *42*(10), 3575–3581. https://doi.org/10.1021/es702880a

Gaillardet, J., Calmels, D., Romero-Mujalli, G., Zakharova, E., & Hartmann, J. (2019). Global climate control on carbonate weathering intensity. *Chemical Geology*, *527*, 118762. https://doi.org/10.1016/j.chemgeo.2018.05.009

Hagmaier, J. L. (1971). *Groundwater flow, hydrochemistry, and uranium deposition in the Powder River Basin, Wyoming* [Doctoral dissertation, University of North Dakota]. https://commons.und.edu/theses/115/?utm_source=commons.und.edu%2Ftheses%2F115&utm_medium=PDF&utm_campaign=PDFCoverPages

Harrison, A. L., Dipple, G. M., Song, W., Power, I. M., Mayer, K. U., Beinlich, A., & Sinton, D. (2017). Changes in mineral reactivity driven by pore fluid mobility in partially wetted porous media. *Chemical Geology*, *463*, 1–11. https://doi.org/10.1016/j.chemgeo.2017.05.003

Hassellöv, M., & von der Kammer, F. (2008). Iron Oxides as Geochemical Nanovectors for Metal Transport in Soil-River Systems. *Elements*, *4*(6), 401–406. https://doi.org/10.2113/gselements.4.6.401

Hatje, V., Payne, T. E., Hill, D. M., McOrist, G., Birch, G. F., & Szymczak, R. (2003). Kinetics of trace element uptake and release by particles in estuarine waters: Effects of pH, salinity, and particle loading. *Environment International*, *29*(5), 619–629. https://doi.org/10.1016/S0160-4120(03)00049-7

Healy, R. W., Rice, C. A., Bartos, T. T., & McKinley, M. P. (2008). Infiltration from an impoundment for coal-bed natural gas, Powder River Basin, Wyoming: Evolution of water and sediment chemistry. *Water Resources Research*, *44*(6). https://doi.org/10.1029/2007WR006396

Hem, J. D., & Cropper, W. H. (1962). *Chemistry of Iron in Natural Water* (USGS Numbered Series No. 1459; Geological Survey Water-Supply Paper). U.S. Geological Survey. https://doi.org/10.3133/wsp1459A

Hochella, M. F., Lower, S. K., Maurice, P. A., Penn, R. L., Sahai, N., Sparks, D. L., & Twining, B. S. (2008). Nanominerals, Mineral Nanoparticles, and Earth Systems. *Science*, *319*(5870), 1631–1635. https://doi.org/10.1126/science.1141134

Hochella, M. F., Mogk, D. W., Ranville, J., Allen, I. C., Luther, G. W., Marr, L. C., McGrail, B. P., Murayama, M., Qafoku, N. P., Rosso, K. M., Sahai, N., Schroeder, P. A., Vikesland, P., Westerhoff, P., & Yang, Y. (2019). Natural, incidental, and engineered

nanomaterials and their impacts on the Earth system. *Science*, *363*(6434), eaau8299. https://doi.org/10.1126/science.aau8299

Horan, K. (2018). *The oxidative weathering of organic matter and its carbon dioxide emissions: Insight from the trace elements rhenium and molybdenum* [Doctoral, Durham University]. http://etheses.dur.ac.uk/12663/

Hoy, R. N., Ogle, K. M., & Taylor, M. (2003). *Evaluation of Water Quality Conditions in Coal Mine Backfill in the Powder River Basin of Wyoming*. 426–447. https://doi.org/10.21000/JASMR03010427

Hu, G., Dam-Johansen, K., Wedel, S., & Hansen, J. P. (2006). Decomposition and oxidation of pyrite. *Progress in Energy and Combustion Science*, *32*(3), 295–314. https://doi.org/10.1016/j.pecs.2005.11.004

Journet, E., Desboeufs, K. V., Caquineau, S., & Colin, J.-L. (2008). Mineralogy as a critical factor of dust iron solubility. *Geophysical Research Letters*, *35*(7). https://doi.org/10.1029/2007GL031589

Jun, Y.-S., Lee, B., & Waychunas, G. A. (2010). In Situ Observations of Nanoparticle Early Development Kinetics at Mineral−Water Interfaces. *Environmental Science & Technology*, *44*(21), 8182–8189. https://doi.org/10.1021/es101491e

Kolker, A., Mroczkowski, S. J., Palmer, C. A., Dennen, K. O., Finkelman, R. B., & Bullock, J. H. (2002). *Toxic Substances From Coal Combustion- A Comprehensive Assessment, Phase II: Element Modes of Occurrence for the Ohio 5/6/7, Wyodak and North Dakota Coal Samples. Final Technical Report* (USGS Numbered Series No. 2002–224; Open-File Report, p. 79). U.S. Geological Survey. https://doi.org/10.3133/ofr02224

Langman, J. B., Blowes, D. W., Veeramani, H., Wilson, D., Smith, L., Sego, D. C., & Paktunc, D. (2015). The mineral and aqueous phase evolution of sulfur and nickel with weathering of pyrrhotite in a low sulfide, granitic waste rock. *Chemical Geology*, *401*, 169–179. https://doi.org/10.1016/j.chemgeo.2015.02.024

Lapakko, K. A., & White, W. W. (2000, January). Modification of the ASTM 5744-96 Kinetic Test. *Proceedings from the 5th International Conference on Acid Rock Drainage*. International Conference on Acid Rock Drainage, Littleton, Colorado. https://www.researchgate.net/publication/284026261_Modification_of_the_ASTM_5744-96_Kinetic_Test

Lasaga, A. C. (1984). Chemical kinetics of water-rock interactions. *Journal of Geophysical Research: Solid Earth*. https://doi.org/10.1029/JB089iB06p04009Li

Lee, R. W. (1980). Geochemistry of water in the Fort Union Formation of the northern Powder River basin, southeastern Montana. In *Geochemistry of water in the Fort Union Formation of the northern Powder River basin, southeastern Montana* (USGS

Numbered Series No. 80–336; Open-File Report, Vols. 80–336). U.S. Geological Survey,. https://doi.org/10.3133/ofr80336

Lehmann, N., Lantuit, H., Böttcher, M. E., Hartmann, J., Eulenburg, A., & Thomas, H. (2022). Alkalinity generation from carbonate weathering in a silicate-dominated headwater catchment at Iskorasfjellet, northern Norway. *Biogeosciences Discussions*, 1–39. https://doi.org/10.5194/bg-2022-205

Li, W., Liu, X.-M., Hu, Y., Teng, F.-Z., & Hu, Y. (2021). Potassium isotopic fractionation during clay adsorption. *Geochimica et Cosmochimica Acta*, *304*, 160–177. https://doi.org/10.1016/j.gca.2021.04.027

Li, X., Zhou, J., Zhou, T., Li, Z., Hu, P., Luo, Y., Christie, P., & Wu, L. (2022). Potential mobilization of cadmium and zinc in soils spiked with smithsonite and sphalerite under different water management regimes. *Journal of Environmental Management*, *324*, 116336. https://doi.org/10.1016/j.jenvman.2022.116336

Liang, L., & Morgan, J. J. (1990). Chemical aspects of iron oxide coagulation in water: Laboratory studies and implications for natural systems. *Aquatic Sciences*, *52*(1), 32–55. https://doi.org/10.1007/BF00878240

Lorenz, J. C., & Nadon, G. C. (2002). Braided-River Deposits in A Muddy Depositional Setting: The Molina Member of the Wasatch Formation (Paleogene), West-Central Colorado, U.S.A. *Journal of Sedimentary Research*, *72*, 376–385. https://doi.org/10.1306/100801720376

Malmström, M., & Banwart, S. (1997). Biotite dissolution at 25°C: The pH dependence of dissolution rate and stoichiometry. *Geochimica et Cosmochimica Acta*, *61*(14), 2779–2799. https://doi.org/10.1016/S0016-7037(97)00093-8

Malmström, M. E., Destouni, G., Banwart, S. A., & Strömberg, B. H. E. (2000). Resolving the Scale-Dependence of Mineral Weathering Rates. *Environmental Science & Technology*, *34*(7), 1375–1378. https://doi.org/10.1021/es990682u

McClurg, J. E. (1988). *Peat forming wetlands and the thick Powder River Basin coals*. 229–236.

Milligan, C., & Reddy, K. (2007). Monitoring of Groundwater Contamination by Trace Elements from CBNG Disposal Ponds Across the Powder River Basin, Wyoming. *Journal American Society of Mining and Reclamation*, *2007*. https://doi.org/10.21000/JASMR07010520

Moore, T. A. (1991). The effects of clastic sedimentation on organic facies development within a Tertiary subbituminous coal bed, Powder River Basin, Montana, U.S.A. *International Journal of Coal Geology*, *18*(3), 187–209. https://doi.org/10.1016/0166-5162(91)90050-S

Nordstrom, D. K., Reitner, J., & Thiel, V. (2011). Sulfide Mineral Oxidation. In *Encyclopedia of Geobiology* (pp. 856–858). Springer Netherlands. http://pubs.er.usgs.gov/publication/70019098

Palmer, C. A., Kolker, A., Finkelman, R. B., Kolb, K. C., Mroozkowski, S. J., Crowley, S. S., Belkin, H. E., Bullock, J., & Motooka, J. M. (1997). *Trace Elements in Coal—Modes of Ocurrence Analysis.* (DOE/PC/95156-04). Minerals Management Service, Reston, VA (United States). https://doi.org/10.2172/644624

Palmer, C. A., Mroozkowski, S. J., Kolker, A., Finkelman, R. B., & Bullock, J. H. (2001). *Chemical analysis and modes of occurrence of selected trace elements in a Powder River basin coal and its corresponding simulated cleaned coal* (USGS Numbered Series No. 2000–323; Open-File Report). U.S. Geological Survey. https://doi.org/10.3133/ofr00323

Paydary, P., Schellenger, A. E. P., Teli, M., Jaisi, D. P., Onnis-Hayden, A., & Larese-Casanova, P. (2021). Chemical oxidation of selenite to selenate: Evaluation of reactive oxygen species and O transfer pathways. *Chemical Geology*, *575*, 120229. https://doi.org/10.1016/j.chemgeo.2021.120229

Perret, D., Gaillard, J.-F., Dominik, J., & Atteia, O. (2000). The Diversity of Natural Hydrous Iron Oxides. *Environmental Science & Technology*, *34*(17), 3540–3546. https://doi.org/10.1021/es0000089

Pocknall, D. T. (1987). Paleoenvironments and age of the Wasatch Formation (Eocene), Powder River basin, Wyoming. *PALAIOS*, *2*, 386–375. https://doi.org/10.2307/3514762

Possemiers, M., Huysmans, M., Anibas, C., Batelaan, O., & Van Steenwinkel, J. (2016). Reactive transport modeling of redox processes to assess Fe(OH)3 precipitation around aquifer thermal energy storage wells in phreatic aquifers. *Environmental Earth Sciences*, *75*(8), 648. https://doi.org/10.1007/s12665-016-5398-7

Rice, C. A., Flores, R. M., Stricker, G. D., & Ellis, M. S. (2008). Chemical and stable isotopic evidence for water/rock interaction and biogenic origin of coalbed methane, Fort Union Formation, Powder River basin, Wyoming and Montana USA. *International Journal of Coal Geology*, *76*. https://doi.org/10.1016/j.coal.2008.05.002

Roehler, H. W. (1987). *Geologic Investigations of the Vermillion Creek Coal Bed in the Eocene Niland Tongue of the Wasatch Formation, Sweetwater County, Wyoming* (pp. 1–25). U.S. Geological Survey. https://books.google.com/books?hl=en&lr=&id=lyXwAAAAMAAJ&oi=fnd&pg=PA25&dq=wasatch+formation+geology+paleoenvironment&ots=ik1_0ziIgH&sig=yw7tpN8upse88rq_BzCy7LMdNmM#v=onepage&q=wasatch%20formation%20geology%20paleoenvironment&f=false

Roehler, H. W. (1991). *Revised stratigraphic nomenclature for the Wasatch and Green River Formations of Eocene age, Wyoming, Utah, and Colorado* (USGS Numbered Series

No. 1506; Professional Paper, p. 38). U.S. Geological Survey. https://doi.org/10.3133/pp1506B

Salmon, S. U., & Malmström, M. E. (2006). Quantification of mineral dissolution rates and applicability of rate laws: Laboratory studies of mill tailings. *Applied Geochemistry*, *21*(2), 269–288. https://doi.org/10.1016/j.apgeochem.2005.09.014

Schwertmann, U. (1991). Solubility and dissolution of iron oxides. *Plant and Soil*, *130*(1), 1–25. https://doi.org/10.1007/BF00011851

See, R. B., Reddy, K. J., Vance, G. F., & Blaylock, M. J. (1995). *Geochemical processes and the effects of natural organic solutes on the solubility of selenium in coal-mine backfill samples from the Powder River Basin, Wyoming* (Water-Resources Investigations Report No. 95–4200). U.S. Geological Survey. https://doi.org/10.3133/wri954200

Sharma, V., Filip, J., Zboril, R., & S. Varma, R. (2015). Natural inorganic nanoparticles – formation, fate, and toxicity in the environment. *Chemical Society Reviews*, *44*(23), 8410–8423. https://doi.org/10.1039/C5CS00236B

Skorina, T., & Allanore, A. (2015). Aqueous alteration of potassium-bearing aluminosilicate minerals: From mechanism to processing. *Green Chemistry*, *17*(4), 2123–2136. https://doi.org/10.1039/C4GC02084G

Slagle, S. E., Lewis, B., & Lee, R. (1985). *Ground-water resources and potential hydrologic effects of surface coal mining in the northern Powder River basin, southeastern Montana* (USGS Numbered Series No. 2239; Water Supply Paper). U.S. Geological Survey. https://doi.org/10.3133/wsp2239

Sparks, D. L. (1991). Chemical Kinetics and Mass Transfer Processes in Soils and Soil Constituents. In J. Bear & M. Y. Corapcioglu (Eds.), *Transport Processes in Porous Media* (pp. 583–637). Springer Netherlands. https://doi.org/10.1007/978-94-011-3628-0_12

St-Arnault, M., Vriens, B., Blaskovich, R., Aranda, C., Klein, B., Ulrich Mayer, K., & Beckie, R. D. (2020). Geochemical and mineralogical assessment of reactivity in a full-scale heterogeneous waste-rock pile. *Minerals Engineering*, *145*, 106089. https://doi.org/10.1016/j.mineng.2019.106089

Stillings, L. L. (2017). Selenium. In *Selenium* (USGS Numbered Series No. 1802-Q; Professional Paper, Vols. 1802-Q, p. 68). U.S. Geological Survey. https://doi.org/10.3133/pp1802Q

Stockwell, J., Smith, L., Jambor, J. L., & Beckie, R. (2006). The relationship between fluid flow and mineral weathering in heterogeneous unsaturated porous media: A physical and geochemical characterization of a waste-rock pile. *Applied Geochemistry*, *21*(8), 1347–1361. https://doi.org/10.1016/j.apgeochem.2006.03.015

Stoeppler, M. (1992). Chapter 8—Cadmium. In M. Stoeppler (Ed.), *Techniques and Instrumentation in Analytical Chemistry* (Vol. 12, pp. 177–230). Elsevier. https://doi.org/10.1016/S0167-9244(08)70107-0

Sun, H., Chen, M., Zou, L., Shu, R., & Ruan, R. (2015). Study of the kinetics of pyrite oxidation under controlled redox potential. *Hydrometallurgy*, *155*, 13–19. https://doi.org/10.1016/j.hydromet.2015.04.003

Torres, J., Pintos, V., Gonzatto, L., Domínguez, S., Kremer, C., & Kremer, E. (2011). Selenium chemical speciation in natural waters: Protonation and complexation behavior of selenite and selenate in the presence of environmentally relevant cations. *Chemical Geology*, *288*(1), 32–38. https://doi.org/10.1016/j.chemgeo.2011.06.015

United States Geological Survey. (1999). *Powder River Basin boundary, 1999 Coal Resource Assessment (prbbndg.shp)* [Data set]. U.S. Geological Survey. https://doi.org/10.5066/P921GQ9R

United States Geological Survey. (2006). Chapter A4. Collection of water samples. In *Chapter A4. Collection of water samples* (USGS Numbered Series No. 09-A4; Techniques of Water-Resources Investigations, Vols. 09-A4, p. 231). U.S. Geological Survey. https://doi.org/10.3133/twri09A4

Wang, H., Jiang, R., Wang, B., & Yao, S. (2021). The Effect of Gypsum on the Fixation of Selenium in the Iron/Calcium-Selenium Coprecipitation Process. *Bulletin of Environmental Contamination and Toxicology*, *106*(1), 121–125. https://doi.org/10.1007/s00128-020-02881-2

Wang, Z., Li, R., Cui, L., Fu, H., Lin, J., & Chen, J. (2018). Characterization and acid-mobilization study for typical iron-bearing clay mineral. *Journal of Environmental Sciences*, *71*, 222–232. https://doi.org/10.1016/j.jes.2018.04.012

Weber, F.-A., Hofacker, A. F., Voegelin, A., & Kretzschmar, R. (2010). Temperature Dependence and Coupling of Iron and Arsenic Reduction and Release during Flooding of a Contaminated Soil. *Environmental Science & Technology*, *44*(1), 116–122. https://doi.org/10.1021/es902100h

White, A. F., Blum, A. E., Schulz, M. S., Bullen, T. D., Harden, J. W., & Peterson, M. L. (1996). Chemical weathering rates of a soil chronosequence on granitic alluvium: I. Quantification of mineralogical and surface area changes and calculation of primary silicate reaction rates. *Geochimica et Cosmochimica Acta*, *60*(14), 2533–2550. https://doi.org/10.1016/0016-7037(96)00106-8

White, A. F., & Brantley, S. L. (1995). Chemical weathering rates of silicate minerals: An overview. In *Chemical Weathering Rates of Silicate Minerals* (pp. 1–22). De Gruyter. https://doi.org/10.1515/9781501509650-003

Williamson, M. A., & Rimstidt, J. D. (1994). The kinetics and electrochemical rate-determining step of aqueous pyrite oxidation. *Geochimica et Cosmochimica Acta*, *58*(24), 5443–5454. https://doi.org/10.1016/0016-7037(94)90241-0

Wunderly, M. D., Blowes, D. W., Frind, E. O., & Ptacek, C. J. (1996). Sulfide mineral oxidation and subsequent reactive transport of oxidation products in mine tailings impoundments: A numerical model. *Water Resources Research*, *32*(10), 3173–3187. https://doi.org/10.1029/96WR02105

Wyoming State Engineer's Office. (1995). *Fort Union Formation Aquifer Monitoring Plan and Preliminary Aquifer Management Plan*. Wyoming Water Development Commission. http://library.wrds.uwyo.edu/wwdcrept/Gillette/Gillette-Ft_Union_Formation_Aquifer_Monitoring_Preliminary_Management_Plan-Final_Rpt-1995.pdf

Yoo, K., & Mudd, S. M. (2008, January 1). *Discrepancy between mineral residence time and soil age: Implications for the interpretation of chemical weathering rates | Geology | GeoScienceWorld*. Geoscience World. https://pubs.geoscienceworld.org/gsa/geology/article-abstract/36/1/35/129993/Discrepancy-between-mineral-residence-time-and?redirectedFrom=fulltext

Yudovich, Ya. E., & Ketris, M. P. (2006). Selenium in coal: A review. *International Journal of Coal Geology*, *67*(1), 112–126. https://doi.org/10.1016/j.coal.2005.09.003

Yuretich, R. F., Hickey, L. J., Gregson, B. P., & Hsia, Y. L. (1984). Lacustrine Deposits in the Paleocene Fort Union Formation, Northern Bighorn Basin, Montana. *Journal of Sedimentary Research*, *54*(3), 836–852. https://doi.org/10.1306/212F8512-2B24-11D7-8648000102C1865D

Appendix A: Supplementary Data

Table A.1 The warm-room ASL elemental concentration data used in figures.

Reporting units	µg/L	µg/L	mg/L	µg/L	mg/L	µg/L	µg/L	µg/L	mg/L	µg/L	mg/L	µg/L	µg/L	µg/L	mg/L	µg/L	mg/L	µg/L
	Total						**0.45-µm filtered**						**0.2-µm filtered**					
Date	**As**	**Cd**	**Ca**	**Fe**	**K**	**Se**	**As**	**Cd**	**Ca**	**Fe**	**K**	**Se**	**As**	**Cd**	**Ca**	**Fe**	**K**	**Se**
12-13-2021	0	0	0	0	0	0	0	0	0	0	0	0	0	0	0	0	0	0
12-16-2021	2.4	1.4	650	2,000	73	580	2.4	1.3	650	<100	73	580	2.4	1.3	620	< 100	73	580
12-20-2021	2.6	1	550	300	60	190	2.1	< 1.0	550	300	60	190	2.1	< 1.0	550	300	60	190
12-23-2021	3.1	< 1.0	560	1,100	55	11	2.4	< 1.0	560	490	55	11	2.4	< 1.0	540	470	52	11
12-27-2021	6	< 1.0	490	2,100	46	2	5.8	< 1.0	460	2,000	44	2	5.6	< 1.0	440	2000	44	2
12-30-2021	6.9	< 1.0	430	1,700	38	1.3	5.8	< 1.0	430	1,500	38	1.3	5.7	< 1.0	430	1500	38	1.2
01-03-2022	6.1	< 1.0	370	1,700	32	< 1.0	5.8	< 1.0	350	1,700	32	< 1.0	5.8	< 1.0	350	1700	32	< 1.0
01-06-2022	5.9	< 1.0	300	1,600	29	< 1.0	4.5	< 1.0	300	1,400	27	< 1.0	4.4	< 1.0	300	1400	25	< 1.0
01-10-2022	5.7	< 1.0	270	1,500	25	< 1.0	4.4	< 1.0	270	1,300	25	< 1.0	4.3	< 1.0	250	1300	23	< 1.0
01-13-2022	4.7	< 1.0	150	1,000	19	< 1.0	4.1	< 1.0	150	870	19	< 1.0	4.1	< 1.0	150	860	18	< 1.0
01-17-2022	5.5	< 1.0	110	860	16	< 1.0	3.9	< 1.0	110	650	16	< 1.0	3.9	< 1.0	110	650	15	< 1.0
01-20-2022	5.1	< 1.0	81	680	13	< 1.0	3.6	< 1.0	81	590	13	< 1.0	3.6	< 1.0	83	590	13	< 1.0
01-24-2022	5	< 1.0	76	720	13	< 1.0	3.5	< 1.0	76	600	13	< 1.0	3.5	< 1.0	76	600	13	< 1.0
01-27-2022	3.8	< 1.0	72	800	12	< 1.0	3.6	< 1.0	72	560	12	< 1.0	3.6	< 1.0	72	560	12	< 1.0
01-31-2022	4.5	< 1.0	69	830	12	< 1.0	3.6	< 1.0	69	620	12	< 1.0	3.6	< 1.0	69	620	12	< 1.0
02-03-2022	4	< 1.0	66	770	12	< 1.0	3.6	< 1.0	63	480	11	< 1.0	3.5	< 1.0	63	460	11	< 1.0
02-07-2022	4.3	< 1.0	63	790	11	< 1.0	3.6	< 1.0	62	520	11	< 1.0	3.5	< 1.0	62	470	11	< 1.0
02-10-2022	4.3	< 1.0	62	730	11	< 1.0	3.5	< 1.0	61	470	10	< 1.0	3.4	< 1.0	61	390	11	< 1.0
02-14-2022	4.6	< 1.0	62	740	11	< 1.0	3.5	< 1.0	59	440	10	< 1.0	3.5	< 1.0	59	430	11	< 1.0
02-17-2022	4.5	< 1.0	58	680	10	< 1.0	3.3	< 1.0	58	450	10	< 1.0	3.3	< 1.0	58	380	10	< 1.0
02-21-2022	4.5	< 1.0	60	710	10	< 1.0	3.4	< 1.0	60	610	10	< 1.0	3.3	< 1.0	55	360	9.5	< 1.0

Table A.1 continued.

02-24-2022	4	< 1.0	55	710	9.7	< 1.0	3.5	< 1.0	55	580	9.7	< 1.0	3.4	< 1.0	55	480	9.7	< 1.0
02-28-2022	4	< 1.0	55	700	9.6	< 1.0	3.4	< 1.0	54	370	9.6	< 1.0	3.3	< 1.0	54	360	9.6	< 1.0
03-07-2022	3.7	< 1.0	53	670	9.1	< 1.0	3	< 1.0	51	370	8.5	< 1.0	3	< 1.0	51	350	8.5	< 1.0
03-14-2022	3.6	< 1.0	51	600	8.6	< 1.0	2.7	< 1.0	50	330	8.2	< 1.0	2.7	< 1.0	50	310	8.2	< 1.0
03-21-2022	3.2	< 1.0	49	540	8.1	< 1.0	3.2	< 1.0	49	280	7.8	< 1.0	3.2	< 1.0	49	260	7.9	< 1.0
03-29-2022	3.3	< 1.0	48	560	7.8	< 1.0	3.3	< 1.0	49	310	7.8	< 1.0	3.2	< 1.0	49	280	7.8	< 1.0
04-05-2022	3.4	< 1.0	49	580	7.7	< 1.0	3.2	< 1.0	47	320	7.5	< 1.0	3.2	< 1.0	46	290	7.4	< 1.0
04-11-2022	3.2	< 1.0	44	550	7.6	< 1.0	3.2	< 1.0	49	260	7.6	< 1.0	3	< 1.0	49	220	7.6	< 1.0
04-18-2022	3.1	< 1.0	41	500	6.9	< 1.0	3.1	< 1.0	45	310	6.9	< 1.0	3.1	< 1.0	41	310	6.4	< 1.0
04-25-2022	3.1	< 1.0	43	510	6.4	< 1.0	3.1	< 1.0	41	290	6	< 1.0	3.1	< 1.0	40	290	6	< 1.0

Table A.2 The warm-room ASL elemental concentration data.

Reporting units	µg/L	µg/L	mg/L	µg/L	mg/L	µg/L	µg/L	µg/L	mg/L	µg/L	mg/L	µg/L	µg/L	µg/L	mg/L	µg/L	mg/L	µg/L
	Total						**0.45-µm filtered**						**0.2-µm filtered**					
Date	**As**	**Cd**	**Ca**	**Fe**	**K**	**Se**	**As**	**Cd**	**Ca**	**Fe**	**K**	**Se**	**As**	**Cd**	**Ca**	**Fe**	**K**	**Se**
12-13-2021	0	0	0	0	0	0	0	0	0	0	0	0	0	0	0	0	0	0
12-16-2021	3	1.1	550	580	57	720	2.3	1.1	550	< 100	57	720	2.3	1.1	540	100	57	670
12-20-2021	1.7	< 1.0	490	< 100	49	120	1.7	< 1.0	490	< 100	49	120	1.6	< 1.0	490	< 100	49	120
12-23-2021	2	< 1.0	490	< 100	46	40	1.4	< 1.0	490	< 100	46	40	1.4	< 1.0	480	< 100	45	40
12-27-2021	1.3	< 1.0	480	140	41	20	1.3	< 1.0	440	< 100	39	20	1.2	< 1.0	440	< 100	39	20
12-30-2021	2.2	< 1.0	460	< 100	37	15	1.1	< 1.0	460	< 100	37	15	1	< 1.0	460	< 100	37	15
01-03-2022	2.4	< 1.0	410	< 100	31	11	< 1.0	< 1.0	400	< 100	31	11	1	< 1.0	400	< 100	31	11
01-06-2022	2.1	< 1.0	360	< 100	27	7.9	< 1.0	< 1.0	360	< 100	27	7.9	< 1.0	< 1.0	340	< 100	25	7.2
01-10-2022	1.9	< 1.0	270	< 100	20	4.9	< 1.0	< 1.0	270	< 100	20	4.8	< 1.0	< 1.0	240	< 100	20	4.8
01-13-2022	2.6	< 1.0	120	< 100	13	3	< 1.0	< 1.0	120	< 100	13	3	< 1.0	< 1.0	120	< 100	13	3.0
01-17-2022	2.1	< 1.0	81	< 100	12	2	< 1.0	< 1.0	81	110	12	1.9	< 1.0	< 1.0	79	< 100	11	1.9
01-20-2022	2.2	< 1.0	70	150	11	1.8	< 1.0	< 1.0	70	110	11	1.8	< 1.0	< 1.0	70	110	11	1.8
01-24-2022	2.2	< 1.0	69	140	11	1.7	< 1.0	< 1.0	69	120	11	1.7	< 1.0	< 1.0	68	110	11	1.7
01-27-2022	1.4	< 1.0	66	180	11	1.6	< 1.0	< 1.0	64	150	10	1.6	< 1.0	< 1.0	64	120	10	1.6
01-31-2022	1.4	< 1.0	64	180	11	1.3	< 1.0	< 1.0	61	170	10	1.3	< 1.0	< 1.0	61	150	10	1.3
02-03-2022	1.2	< 1.0	63	200	11	1.3	< 1.0	< 1.0	59	190	10	1.3	< 1.0	< 1.0	59	150	9.9	1.3
02-07-2022	1.3	< 1.0	62	250	10	1.2	< 1.0	< 1.0	59	150	9.7	1.2	< 1.0	< 1.0	59	190	9.7	1.2

Table A.2 continued.

02-10-2022	1.9	< 1.0	60	250	9.8	1.1	< 1.0	< 1.0	56	110	9.5	1	< 1.0	< 1.0	56	140	9.4	1
02-14-2022	1.7	< 1.0	58	210	9.9	1.1	< 1.0	< 1.0	58	120	9.9	< 1.0	< 1.0	< 1.0	58	< 100	9.8	< 1.0
02-17-2022	1.5	< 1.0	57	170	9.5	< 1.0	< 1.0	< 1.0	57	160	9.5	< 1.0	< 1.0	< 1.0	57	130	9.5	< 1.0
02-21-2022	1.7	< 1.0	57	180	9.5	< 1.0	< 1.0	< 1.0	56	160	9.5	< 1.0	< 1.0	< 1.0	55	110	9.2	< 1.0
02-24-2022	< 1.0	< 1.0	51	180	9	< 1.0	< 1.0	< 1.0	50	110	8.8	< 1.0	< 1.0	< 1.0	50	120	8.6	< 1.0
02-28-2022	< 1.0	< 1.0	53	150	9.2	< 1.0	< 1.0	< 1.0	52	110	9.2	< 1.0	< 1.0	< 1.0	52	110	8.9	< 1.0
03-07-2022	< 1.0	< 1.0	51	< 100	9.1	< 1.0	< 1.0	< 1.0	51	< 100	9.1	< 1.0	< 1.0	< 1.0	53	< 100	9.1	< 1.0
03-14-2022	< 1.0	< 1.0	47	< 100	8.3	< 1.0	< 1.0	< 1.0	47	< 100	8.3	< 1.0	< 1.0	< 1.0	47	< 100	8.3	< 1.0
03-21-2022	< 1.0	< 1.0	46	< 100	8.3	< 1.0	< 1.0	< 1.0	46	< 100	8.3	< 1.0	< 1.0	< 1.0	46	< 100	8.1	< 1.0
03-29-2022	< 1.0	< 1.0	46	< 100	8.2	< 1.0	< 1.0	< 1.0	46	< 100	8.2	< 1.0	< 1.0	< 1.0	45	< 100	8.1	< 1.0
04-05-2022	< 1.0	< 1.0	42	< 100	7.7	< 1.0	< 1.0	< 1.0	42	< 100	7.7	< 1.0	< 1.0	< 1.0	41	< 100	7.6	< 1.0
04-11-2022	< 1.0	< 1.0	44	< 100	7.8	< 1.0	< 1.0	< 1.0	44	< 100	7.8	< 1.0	< 1.0	< 1.0	44	< 100	7.8	< 1.0
04-18-2022	< 1.0	< 1.0	37	< 100	6.8	< 1.0	< 1.0	< 1.0	37	< 100	6.8	< 1.0	< 1.0	< 1.0	37	< 100	6.8	< 1.0
04-25-2022	< 1.0	< 1.0	37	< 100	6.7	< 1.0	< 1.0	< 1.0	37	< 100	6.4	< 1.0	< 1.0	< 1.0	37	< 100	6.5	< 1.0

Table A.3 Warm-room unfiltered elemental concentration data input into the principal component analysis.

Reporting Units	µg/L	µg/L	µg/L	mg/L	µg /L	mg/L	µg/L	µg/L	µg /L	mg/L	µg /L
Date	As	Ba	B	Ca	Fe	Mg	Mn	Mo	Ni	K	Zn
12-13-2021	0	0	0	0	0	0	0	0	0	0	0
12-16-2021	2.4	64	810	650	2000	410	2200	3.2	83	73	120
12-20-2021	2.6	45	730	550	300	310	2400	2	60	60	130
12-23-2021	3.1	42	670	560	1100	280	2700	1.6	57	55	75
12-27-2021	6	39	990	490	2100	220	2600	1.4	44	46	63
12-30-2021	6.9	49	750	430	1700	180	2500	1.5	37	38	55
01-03-2022	6.1	57	680	370	1700	150	2400	1.4	35	32	53
01-06-2022	5.9	58	810	300	1600	120	1800	1.3	37	29	39
01-10-2022	5.7	70	440	270	1500	98	1400	1.3	23	25	28
01-13-2022	4.7	82	410	150	1000	53	880	1.3	21	19	24
01-17-2022	5.5	110	340	110	860	39	590	1.3	15	16	43
01-20-2022	5.1	120	330	83	680	27	430	1.4	13	13	11
01-24-2022	5	150	270	76	720	24	390	1.5	13	13	11
01-27-2022	3.8	150	390	72	800	23	380	1.5	11	12	<10
01-31-2022	4.5	160	200	69	830	22	370	1.6	11	12	15
02-03-2022	4	160	220	66	770	21	350	1.6	12	12	12
02-07-2022	4.3	170	300	63	790	20	340	1.7	11	11	<10
02-10-2022	4.3	180	360	62	730	20	360	1.8	11	11	<10
02-14-2022	4.6	180	420	62	740	20	350	1.7	11	11	16
02-17-2022	4.5	180	250	58	680	19	330	1.9	11	10	<10
02-21-2022	4.5	180	210	60	710	20	330	1.8	10	10	<10
02-24-2022	4	170	360	55	710	18	290	2	<10	9.7	<10
02-28-2022	4	170	290	55	700	18	300	3	<10	9.6	<10
03-07-2022	3.7	170	450	53	670	18	290	2.1	<10	9.1	<10
03-14-2022	3.6	160	750	51	600	17	280	2.1	<10	8.6	<10
03-21-2022	3.2	160	460	49	540	16	260	2.1	<10	8.1	<10
03-29-2022	3.3	160	620	49	560	16	250	2.1	<10	7.8	<10
04-05-2022	3.4	160	190	49	580	16	260	3.6	<10	7.7	<10
04-11-2022	3.2	150	120	49	550	17	250	2.5	<10	7.6	19
04-18-2022	3.1	150	120	45	500	15	240	2.6	<10	6.9	<10
04-25-2022	3.1	150	190	43	510	15	240	2.8	<10	6.4	<10

Table A.4 Warm-room 0.45-μm filtered elemental concentration data input into the principal component analysis.

Reporting Units	μg/L	μg/L	μg/L	mg/L	μg /L	mg/L	μg/L	μg/L	μg /L	mg/L	μg /L
Date	As	Ba	B	Ca	Fe	Mg	Mn	Mo	Ni	K	Zn
12-13-2021	0	0	0	0	0	0	0	0	0	0	0
12-16-2021	2.4	64	720	650	<100	410	2200	2.9	83	73	120
12-20-2021	2.1	45	650	550	300	310	2400	2	60	60	81
12-23-2021	2.4	42	670	560	490	280	2700	1.5	57	55	69
12-27-2021	5.8	39	500	460	2000	220	2600	1.4	43	44	61
12-30-2021	5.8	49	440	430	1500	180	2500	1.5	37	38	55
01-03-2022	5.8	57	420	350	1700	150	2400	1.4	35	32	53
01-06-2022	4.5	56	310	300	1400	120	1800	1.2	27	27	39
01-10-2022	4.4	68	280	270	1300	98	1400	1.2	23	25	28
01-13-2022	4.1	82	240	150	870	53	880	1.2	21	19	24
01-17-2022	3.9	110	220	110	650	37	590	1.2	13	16	43
01-20-2022	3.6	120	210	83	590	27	430	1.3	13	13	120
01-24-2022	3.5	150	190	76	600	24	390	1.3	12	13	81
01-27-2022	3.6	150	200	72	560	23	380	1.5	11	12	<10
01-31-2022	3.6	160	190	69	620	22	360	1.5	10	12	<10
02-03-2022	3.6	160	170	63	480	20	350	1.6	12	11	<10
02-07-2022	3.6	170	150	62	520	20	340	1.6	11	11	<10
02-10-2022	3.5	170	150	61	470	20	310	1.6	10	11	<10
02-14-2022	3.5	170	140	59	440	19	310	1.5	10	11	12
02-17-2022	3.3	160	120	58	450	19	310	1.9	11	10	<10
02-21-2022	3.4	160	110	60	610	19	310	1.8	10	10	<10
02-24-2022	3.5	170	110	55	580	18	290	1.9	<10	9.7	<10
02-28-2022	3.4	170	100	54	370	18	300	3	<10	9.6	<10
03-07-2022	3	160	110	51	370	17	270	2	<10	8.5	<10
03-14-2022	2.7	160	<100	50	330	17	270	1.9	<10	8.2	<10
03-21-2022	3.2	160	100	49	280	16	250	2.1	<10	7.9	<10
03-29-2022	3.3	160	<100	49	310	16	250	2	<10	7.8	<10
04-05-2022	3.2	150	<100	47	320	16	250	3.6	<10	7.5	<10
04-11-2022	3.2	150	<100	49	260	17	250	2.2	<10	7.6	<10
04-18-2022	3.1	150	<100	45	310	15	240	2.6	<10	6.9	<10
04-25-2022	3.1	140	<100	41	290	14	220	2.7	<10	6	<10

Table A.5 Warm-room 0.2-µm filtered elemental concentration data input into the principal component analysis.

Reporting Units	µg/L	µg/L	µg/L	mg/L	µg /L	mg/L	µg/L	µg/L	µg /L	mg/L	µg /L
Date	As	Ba	B	Ca	Fe	Mg	Mn	Mo	Ni	K	Zn
12-13-2021	0	0	0	0	0	0	0	0	0	0	0
12-16-2021	2.4	63	720	620	<100	390	2200	2.9	82	73	120
12-20-2021	2.1	45	650	550	300	310	2400	2	60	60	81
12-23-2021	2.4	42	670	540	470	280	2700	1.5	57	52	69
12-27-2021	5.6	39	500	440	2000	210	2600	1.4	43	44	61
12-30-2021	5.7	45	440	430	1500	180	2400	1.4	35	38	50
01-03-2022	5.8	57	420	350	1700	140	2400	1.4	35	32	53
01-06-2022	4.4	56	310	300	1400	120	1800	1.1	27	25	38
01-10-2022	4.3	68	280	250	1300	91	1400	1.2	22	23	28
01-13-2022	4.1	82	240	150	860	53	880	1.1	21	18	23
01-17-2022	3.9	110	220	110	650	36	590	1.2	13	15	13
01-20-2022	3.6	120	210	83	590	27	430	1.3	13	13	120
01-24-2022	3.5	150	190	76	600	24	390	1.3	12	13	81
01-27-2022	3.6	140	200	72	560	23	360	1.4	10	12	<10
01-31-2022	3.6	160	190	69	620	22	360	1.5	10	12	<10
02-03-2022	3.5	160	170	63	460	20	340	1.6	12	11	<10
02-07-2022	3.5	170	150	62	470	20	340	1.6	11	11	<10
02-10-2022	3.4	160	150	61	390	20	310	1.5	10	11	<10
02-14-2022	3.5	170	140	59	430	19	310	1.5	10	11	12
02-17-2022	3.3	160	120	58	380	19	310	1.8	11	10	<10
02-21-2022	3.3	160	110	55	360	18	310	1.7	<10	9.5	<10
02-24-2022	3.4	170	110	55	480	18	290	1.8	<10	9.7	<10
02-28-2022	3.3	170	100	54	360	18	300	3	<10	9.6	<10
03-07-2022	3	160	100	51	350	17	270	1.9	<10	8.5	<10
03-14-2022	2.7	160	<100	50	310	17	270	1.9	<10	8.2	<10
03-21-2022	3.2	160	<100	49	260	16	250	2	<10	7.9	<10
03-29-2022	3.2	160	<100	49	280	16	250	2	<10	7.8	<10
04-05-2022	3.2	150	<100	46	290	16	250	2.3	<10	7.4	<10
04-11-2022	3	150	<100	49	220	17	250	2.2	<10	7.6	<10
04-18-2022	3.1	150	<100	41	310	14	240	2.5	<10	6.4	<10
04-25-2022	3.1	140	<100	40	290	14	220	2.6	<10	6	<10

Table A.6 Cold-room unfiltered elemental concentration data input into the principal component analysis.

Reporting Units	µg/L	µg/L	µg/L	mg/L	µg /L	mg/L	µg/L	µg/L	µg /L	mg/L	µg /L
Date	As	Ba	B	Ca	Fe	Mg	Mn	Mo	Ni	K	Zn
12-13-2021	0	0	0	0	0	0	0	0	0	0	0
12-16-2021	3	59	860	550	580	400	1500	2.4	66	57	100
12-20-2021	1.7	35	480	490	<100	310	1700	1.3	46	49	71
12-23-2021	2	32	510	490	<100	280	1600	1.2	35	46	63
12-27-2021	1	31	600	480	140	250	1700	<1	31	41	57
12-30-2021	2.2	30	310	460	<100	220	1700	1.1	31	37	55
01-03-2022	2.4	28	340	410	<100	180	1500	1	28	31	52
01-06-2022	2.1	25	380	360	<100	110	970	1	19	27	29
01-10-2022	1.9	32	370	270	<100	76	600	1.1	15	20	20
01-13-2022	2.6	47	280	120	<100	34	330	1.1	12	13	12
01-17-2022	2.1	68	350	81	<100	20	220	1.2	11	12	13
01-20-2022	2.2	83	490	70	150	18	200	1.2	11	11	<10
01-24-2022	2.2	92	300	69	140	18	200	1.2	10	11	<10
01-27-2022	1.4	90	230	66	180	18	200	1.2	<10	11	16
01-31-2022	1.4	96	240	64	180	17	200	1.2	<10	11	<10
02-03-2022	1.2	96	570	63	200	17	200	1.2	<10	11	<10
02-07-2022	1.3	110	210	62	250	17	210	1.1	<10	10	16
02-10-2022	1.9	110	230	60	250	16	230	1.1	<10	9.8	13
02-14-2022	1.7	120	410	58	210	16	230	0.5	<10	9.9	<10
02-17-2022	1.5	110	230	57	170	15	220	0.5	<10	9.5	<10
02-21-2022	1.7	120	500	57	180	16	220	0.5	<10	9.5	<10
02-24-2022	<1	110	520	51	180	14	210	1.2	<10	9	<10
02-28-2022	<1	120	280	53	150	15	210	1.2	<10	9.2	<10
03-07-2022	<1	110	330	53	<100	15	200	1.3	<10	9.1	<10
03-14-2022	<1	110	400	47	<100	13	190	1.3	<10	8.3	<10
03-21-2022	<1	110	230	46	<100	13	180	1.3	<10	8.3	<10
03-29-2022	<1	120	250	46	<100	13	180	1.2	<10	8.2	<10
04-05-2022	<1	110	370	42	<100	12	180	1.2	<10	7.7	<10
04-11-2022	<1	120	120	44	<100	13	180	1.4	<10	7.8	19
04-18-2022	<1	120	200	37	<100	11	170	1.4	<10	6.8	<10
04-25-2022	<1	120	110	37	<100	11	170	1.5	<10	6.7	<10

Table A.7 Cold-room 0.45-µm filtered elemental concentration data input into the principal component analysis.

Reporting Units	µg/L	µg/L	µg/L	mg/L	µg /L	mg/L	µg/L	µg/L	µg /L	mg/L	µg /L
Date	As	Ba	B	Ca	Fe	Mg	Mn	Mo	Ni	K	Zn
12-13-2021	0	0	0	0	0	0	0	0	0	0	0
12-16-2021	2.3	51	390	550	<100	400	1800	2.3	66	57	95
12-20-2021	1.7	35	330	490	<100	310	1700	1.3	46	49	63
12-23-2021	1.4	32	350	490	<100	280	1600	1.2	34	46	57
12-27-2021	1.3	30	320	440	<100	250	1700	<1	30	39	55
12-30-2021	1.1	30	300	460	<100	220	1700	1.1	31	37	55
01-03-2022	1	28	290	400	<100	180	1500	1	28	31	52
01-06-2022	<1	24	220	360	<100	110	930	<1	19	27	29
01-10-2022	<1	31	210	270	<100	76	570	<1	15	20	20
01-13-2022	<1	47	180	120	<100	34	320	1	11	13	12
01-17-2022	<1	68	180	81	<100	20	220	<1	<10	12	10
01-20-2022	<1	80	180	70	100	18	200	1.1	<10	11	<10
01-24-2022	<1	92	190	69	110	18	190	1.1	<10	11	<10
01-27-2022	<1	90	180	64	110	18	200	1.2	<10	10	<10
01-31-2022	<1	96	170	61	150	17	200	1.2	<10	10	<10
02-03-2022	<1	95	150	59	170	17	200	1.2	<10	10	<10
02-07-2022	<1	100	140	59	180	17	210	1.1	<10	9.7	<10
02-10-2022	<1	98	140	56	150	16	200	1.1	<10	9.5	<10
02-14-2022	<1	110	130	58	110	16	210	0.5	<10	9.9	<10
02-17-2022	<1	110	110	57	130	15	210	<1	<10	9.5	<10
02-21-2022	<1	110	100	56	160	16	210	<1	<10	9.5	<10
02-24-2022	<1	110	100	50	160	14	210	1.1	<10	8.8	<10
02-28-2022	<1	120	100	52	110	15	210	1.1	<10	9.2	<10
03-07-2022	<1	110	<100	53	<100	15	200	1.2	<10	9.1	<10
03-14-2022	<1	100	<100	47	<100	13	190	1.2	<10	8.3	<10
03-21-2022	<1	110	<100	46	<100	13	180	1.3	<10	8.3	<10
03-29-2022	<1	120	<100	46	<100	13	180	1.2	<10	8.2	<10
04-05-2022	<1	110	<100	42	<100	12	180	1.2	<10	7.7	<10
04-11-2022	<1	120	<100	44	<100	13	170	1.2	<10	7.8	<10
04-18-2022	<1	120	<100	37	<100	11	170	1.4	<10	6.8	<10
04-25-2022	<1	120	<100	37	<100	11	170	1.5	<10	6.5	<10

Table A.8 Cold-room 0.2-µm filtered elemental concentration data input into the principal component analysis.

Reporting Units	µg/L	µg/L	µg/L	mg/L	µg /L	mg/L	µg/L	µg/L	µg /L	mg/L	µg /L
Date	As	Ba	B	Ca	Fe	Mg	Mn	Mo	Ni	K	Zn
12-13-2021	0	0	0	0	0	0	0	0	0	0	0
12-16-2021	2.3	51	390	540	<100	400	1800	2.3	66	57	95
12-20-2021	1.6	35	330	490	<100	310	1700	1.3	46	49	63
12-23-2021	1.4	32	350	480	<100	280	1600	1.1	34	45	57
12-27-2021	1.2	30	320	440	<100	240	1700	<1	30	39	55
12-30-2021	1	30	300	460	<100	220	1600	1.1	31	37	55
01-03-2022	1	27	270	400	<100	170	1400	1	27	31	51
01-06-2022	<1	24	220	340	<100	120	920	<1	19	25	29
01-10-2022	<1	31	210	240	<100	76	570	<1	15	20	20
01-13-2022	<1	47	180	120	<100	32	320	1	11	13	12
01-17-2022	<1	67	180	79	<100	20	220	<1	<10	11	<10
01-20-2022	<1	79	170	70	110	18	200	1	<10	11	<10
01-24-2022	<1	91	190	68	110	18	180	1	<10	11	<10
01-27-2022	<1	90	180	64	120	17	200	1.2	<10	10	<10
01-31-2022	<1	96	170	61	150	17	200	1.2	<10	10	<10
02-03-2022	<1	94	150	59	150	16	200	1.2	<10	9.9	<10
02-07-2022	<1	100	140	59	190	16	210	1.1	<10	9.7	<10
02-10-2022	<1	98	140	56	140	15	200	1.1	<10	9.4	<10
02-14-2022	<1	110	130	58	50	16	210	<1	<10	9.8	<10
02-17-2022	<1	110	110	57	130	15	210	<1	<10	9.5	<10
02-21-2022	<1	110	100	55	110	15	210	<1	<10	9.2	<10
02-24-2022	<1	110	100	50	120	14	210	1.1	<10	8.6	<10
02-28-2022	<1	120	100	52	110	14	210	1	<10	8.9	<10
03-07-2022	<1	110	<100	53	<100	15	200	1.2	<10	9.1	<10
03-14-2022	<1	100	<100	47	<100	13	190	1.2	<10	8.3	<10
03-21-2022	<1	110	<100	46	<100	13	180	1.3	<10	8.1	<10
03-29-2022	<1	120	<100	45	<100	13	180	1.2	<10	8.1	<10
04-05-2022	<1	110	<100	41	<100	12	180	1.2	<10	7.6	<10
04-11-2022	<1	120	<100	44	<100	13	170	1.2	<10	7.8	<10
04-18-2022	<1	120	<100	37	<100	11	170	1.4	<10	6.8	<10
04-25-2022	<1	110	<100	37	<100	11	160	1.5	<10	6.5	<10

Table A.9 Field parameter data.

Reporting Units	mV	mV	µS/cm	µS/cm			mg/L	mg/L
Date	Eh-warm	Eh-cold	Conductivity-warm	conductivity-cold	pH-warm	pH-cold	Alkalinity-warm	Alkalinity-cold
12/16/2021	142	154.6	6,410	6,350	6.28	6.47	550	613
12/20/2021	123.7	133.2	4,980	5,010	6.2	6.46	587	632
12/23/2021	45.6	12.8	4,230	4,180	6.27	6.48	395	436.2
12/27/2021	29	-67.2	3,340	3,590	6.21	6.3	348	287
12/30/2021	-109.3	-101.4	2,998	3,150	6.05	6.31	385.9	274.7
1/3/2022	100.4	120.2	2,558	2,710	6.11	6.33	369.5	271.1
1/6/2022	68.1	48.3	2,097	1,934	6.14	6.44	364.5	280.7
1/10/2022	-52.4	-74.2	1,661	1,240	6.16	6.49	357.5	278.8
1/13/2022	54.5	127	1,242	823	6.2	6.55	326.4	278.8
1/17/2022	-113.4	-118.2	835	576	6.22	6.59	341.1	238.3
1/20/2022	-20.8	-20.8	621	485	6.29	6.64	295.7	210.2
1/24/2022	-6	-34.8	566	484	6.31	6.65	258.8	213
1/27/2022	39.1	33.5	540	451	6.32	6.66	249.9	214.5
1/31/2022	52.2	47.5	517	445	6.32	6.66	252.7	181.6
2/3/2022	56.2	50.6	485	421	6.55	6.62	241.3	187.4
2/7/2022	35.9	21.5	481	430	6.51	6.6	223.7	168
2/10/2022	57.5	59.9	461	401	6.61	6.62	231.1	181.4
2/14/2022	31	49.4	458	410	6.52	6.55	220.4	173.2
2/17/2022	-5.4	20	434	396	6.51	6.65	208.2	166
2/21/2022	30.8	52.3	436	392	6.6	6.68	202.2	174.1
2/24/2022	54.1	58.5	424	371	6.59	6.69	173.7	165.6
2/28/2022	42.8	50.9	422	380	6.57	6.72	204.3	165.4
3/3/2022	91.5	95.3	400	394	6.71	6.68	175.5	158.9
3/7/2022	69.3	91	404	371	6.66	6.74	167.1	172.2
3/10/2022	57.4	79.7	394	348	6.72	6.76	187.2	166.7
3/14/2022	45	48.6	389	341	6.57	6.79	176.7	163.7
3/17/2022	76.8	97.3	376	331	6.71	6.78	171.9	164.4
3/21/2022	85.4	94.5	365	325	6.78	6.93	163.9	161.2
3/24/2022	69.1	82	351	316	6.75	6.84	175	155.3
3/28/2022	73.7	83.2	360	316	6.74	6.93	163.7	158.3
3/31/2022	78	92	347	303	6.81	6.9	156.2	155.5
4/4/2022	55.9	76.6	354	296.8	6.84	6.91	162.9	161.8

Table A.9 continued.

4/7/2022	57	66.6	340	287.7	6.85	6.96	171.6	156.6
4/11/2022	83.6	92.9	348	291.5	6.97	7.02	192.1	151.8
4/14/2022	67.5	74.9	333	286.9	7.03	7.04	164	153.6
4/18/2022	54.8	68.7	327	286	6.86	6.88	163.7	149.2
4/21/2022	65.6	75.6	321	276.4	6.83	6.98	152.4	147.4
4/25/2022	59.9	63.8	321	276.3	6.85	6.94	159.3	145.5
4/28/2022	75.3	84.1	315	271.2	6.86	6.96	148.3	139.7

Table A.10 Grain size distribution analysis results.

Grainsize (mm)	Percent Passing				
	Pre-Fort Union	Pre-Wasatch	Post-Low	Post-Middle	Post-High
0.01	0	0	0	0	0
0.02	4.4	0	0.1	0	0
0.038	7.6	0	0.4	0.6	0
0.075	8.1	0.4	5.9	4.5	3
0.15	16.2	4.8	14.8	11.4	10.3
0.3	36.2	12.8	35.2	27.2	25
0.425	50	25.8	45.2	41.2	37.1
0.85	65	52.7	70.2	64.9	61.2
2	82.9	85.5	95.9	95.3	94.7
4.75	98.7	96.3	99.4	99.3	99.4
5.6	100	98.7	100	99.5	99.7
6.3	100	99.5	100	100	100

Table A.11 Waste rock XRF results.

	Weight percent	
Element	Fort Union Formation	Wasatch Formation
SiO2	61.7	82.16
TiO2	0.458	0.171
Al2O3	11.91	8.22
FeO	2.26	1.17
MnO	0.025	0.016
MgO	0.93	0.58
CaO	1.08	0.64
Na2O	0.28	1.09
K2O	2	2.78
P2O5	0.104	0.054